EPJ Plus

EPJ.org
your physics journal

Eur. Phys. J. Plus (2011) **126**: 101 DOI 10.1140/epjp/i2011-11101-2

Methodological challenges in combining quantum-mechanical and continuum approaches for materials science applications

M. Friák, T. Hickel, B. Grabowski, L. Lymperakis, A. Udyansky, A. Dick, D. Ma, F. Roters, L.-F. Zhu, A. Schlieter, U. Kühn, Z. Ebrahimi, R. A. Lebensohn, D. Holec, J. Eckert, H. Emmerich, D. Raabe and J. Neugebauer

Eur. Phys. J. Plus (2011) **126**: 101
DOI 10.1140/epjp/i2011-11101-2

THE EUROPEAN PHYSICAL JOURNAL PLUS

Review

Methodological challenges in combining quantum-mechanical and continuum approaches for materials science applications

M. Friák[1,a], T. Hickel[1], B. Grabowski[1], L. Lymperakis[1], A. Udyansky[1], A. Dick[1], D. Ma[1], F. Roters[1], L.-F. Zhu[1], A. Schlieter[2,3], U. Kühn[2], Z. Ebrahimi[4], R. A. Lebensohn[5], D. Holec[6], J. Eckert[2,3], H. Emmerich[7], D. Raabe[1], and J. Neugebauer[1]

[1] Max-Planck-Institut für Eisenforschung GmbH - Max-Planck-Strasse 1, D-40237, Düsseldorf, Germany
[2] IFW Dresden, Institute for Complex Materials - Helmholtzstr. 20, D-01069 Dresden, Germany
[3] Dresden University of Technology, Institute of Materials Science - D-01062 Dresden, Germany
[4] AICES Graduate School, RWTH Aachen - D-52056, Germany
[5] Materials Science and Technology Division, Los Alamos National Laboratory - Los Alamos, NM 87845, USA
[6] Montanuniversität Leoben - Franz-Josef-Straße 18, A-8700 Leoben, Austria
[7] University Bayreuth - Universitätsstrasse 30, 95440 Bayreuth, Germany

Received: 18 May 2011 / Revised: 25 August 2011
Published online: 27 October 2011 –

Abstract. Multi-methodological approaches combining quantum-mechanical and/or atomistic simulations with continuum methods have become increasingly important when addressing multi-scale phenomena in computational materials science. A crucial aspect when applying these strategies is to carefully check, and if possible to control, a variety of intrinsic errors and their propagation through a particular multi-methodological scheme. The first part of our paper critically reviews a few selected sources of errors frequently occurring in quantum-mechanical approaches to materials science and their multi-scale propagation when describing properties of multi-component and multi-phase polycrystalline metallic alloys. Our analysis is illustrated in particular on the determination of i) thermodynamic materials properties at finite temperatures and ii) integral elastic responses. The second part addresses methodological challenges emerging at interfaces between electronic structure and/or atomistic modeling on the one side and selected continuum methods, such as crystal elasticity and crystal plasticity finite element method (CEFEM and CPFEM), new fast Fourier transforms (FFT) approach, and phase-field modeling, on the other side.

1 Introduction

Modern materials science is based on a structure-property paradigm related to materials hierarchical nature and yields a connection of macroscopic properties over multiple length and time scales. The lowest scale still influencing these materials properties is governed by electrons being responsible for the chemical bonds between atoms. Many promising strategies of condensed matter theory are, therefore, based on the determination of the electronic structure (ES) of the considered materials and an intelligent transfer of its characteristics to higher-order scales using multi-disciplinary schemes. More specifically, if the interaction of electrons is solely described using universal principles such as the fundamental laws of quantum mechanics condensed in the Schrödinger equation, these simulations are called first-principles, or *ab initio* methods.

Unfortunately, a solution of the quantum-mechanical Schrödinger equation including all relevant interactions between the electrons and atomic nuclei in solids is computationally extremely demanding. Consequently, practical ES calculations in solids were rather rare prior to the availability of high-speed computers. Even with increasing computational resources, however, a series of approximations must be employed in order to render a comprehensive solution for any non-trivial system feasible. Despite these limitations it is nowadays not only possible to simulate certain experimental conditions and set-ups at an unprecedented level of accuracy without any experimental input, but also to design new materials with tailored properties before actually casting them.

[a] e-mail: m.friak@mpie.de

One of the most established *ab initio* methods in materials science is the density functional theory (DFT) [1,2], which has developed very rapidly in the last three decades. It has now become a reliable and powerful tool for a vast spectrum of physical, chemical, metallurgical and engineering applications.

DFT is based upon Hohenberg-Kohn theorems [1] which state that i) all the physical properties of a system of interacting electrons are uniquely determined by its ground-state electron density distribution and ii) there exists a universal energy functional that is minimized by the ground-state density. As shown by Kohn and Sham [2], the problem of a system of interacting electrons can be then mapped onto an equivalent non-interacting problem. The ground-state charge-density distribution and the non-interacting kinetic energy functional are given in terms of the auxiliary Kohn-Sham (KS) orbitals and the ground-state energy is expressed in terms of the KS eigenvalues. The KS orbitals are found as solutions of non-linear (Schrödinger-like) equations, where potentials depend on their own eigenfunctions through the electron density distribution. The unknown functional of a system of interacting electrons can be written as a sum of known ground-state kinetic energies of a system of non-interacting electrons, the classical electrostatic self-interaction of the electronic density, and an unknown so-called exchange-correlation (xc) functional. The exchange-correlation energy is the name given to the part of the energy functional that is not known and that must be approximated (*e.g.*, local density approximation (LDA), generalized gradient approximation (GGA), as discussed also below). Once an explicit form for the xc energy is available, the KS equations can be solved in a self-consistent way using a variety of methods. When implemented, the KS orbitals are often expanded into a series of suitable basis functions, localized (such as, for example, atomic orbitals) in case of molecular systems, delocalized (*e.g.*, plane waves) in case of periodic infinite crystals, or their combination. For more information see, *e.g.*, [3–8].

The predictive strength of DFT-based computational approaches can be either used directly to determine scale-independent materials properties (such as the atomic density or the thermal expansion coefficient), or as an input for the up-scale transfer of materials parameters in multi-scale methods. In both cases, possible sources of errors (see, *e.g.*, [9–11]) must be identified, their impact on the obtained results and parameters as well as their scale propagation in multi-methodological schemes (see, *e.g.*, [12]) must be carefully analyzed. This article is intended to indicate a set of common sources of errors in *ab initio* based simulations and to shed more light on possible strategies to keep their impact low.

2 Common errors in computational materials science: Their origin and propagation

From a practical user's point of view different sources of errors connected with *ab initio* computational methods can be classified by the extent to which users can influence them. This is hardly possible for systematic *methodological* and *implementation* errors, reflecting properties of the actual computational method and its implementation in the code used to perform the calculations. The most severe *methodological errors* of DFT are probably i) the approximation inherent to the employed exchange-correlation (xc) functionals and ii) the ground-state character of the DFT. Still there are ongoing developments in order to reduce or even remove these fundamental sources of errors.

As far as *implementation errors* are concerned, one should be aware that the choice of the DFT code implies a selection of certain concepts, *e.g.*, concerning the amount of electrons that are explicitly treated (all-electron *vs.* pseudopotential codes), the choice of either localized or delocalized basis set, or the type of boundary conditions (periodic or not). Again the modification of these sources of errors is mostly due to method developers and they can hardly be eliminated by a user of the code. Consequently, users must carefully choose such a code that is well suited to their problem or must bypass the implemented limitations. For instance, spurious interactions imposed by periodic boundary conditions must be properly addressed when calculating properties of non-ideal crystals with symmetry-breaking defects (surfaces, interfaces and such).

A second class of computational errors are the *numerical* errors related to the setting of convergence parameters that determine the precision of calculated results in the computer. These errors are typically caused by the fact that continuous variables need to be discretized and in principle infinite series expansions need to be truncated in practical calculations. To this class of errors belongs, *e.g.*, the number of reciprocal space k-points in the Brillouin zone over which the code sums the electronic states, the value of the smearing parameter determining the distribution of electronic states close to the Fermi energy, or the cut-off energy that is decisive for the size of the basis set in codes with the plane-wave basis. A larger value for these parameters results typically in a higher precision of the results and at the same time in a larger demand of computational resources. Therefore, the convergence parameters are set such as to find a compromise between the precision and the computational and/or time expenses for the calculations.

In contrast to the first class of errors, the numerical errors are typically under the user's full control. Despite of this fact, the representing values of these parameters should not be underrated because the values of parameters providing the so-called well-converged results often differ from one studied material to another, as well as from one studied property to another, even in the case of the same materials system. As an example, we show in fig. 1 calculation results of convergence tests obtained for single-crystalline elastic constants of α-Fe. The values summarized in the figure illustrate the fact that the calculated values may be at the same time either well matching measured values (see

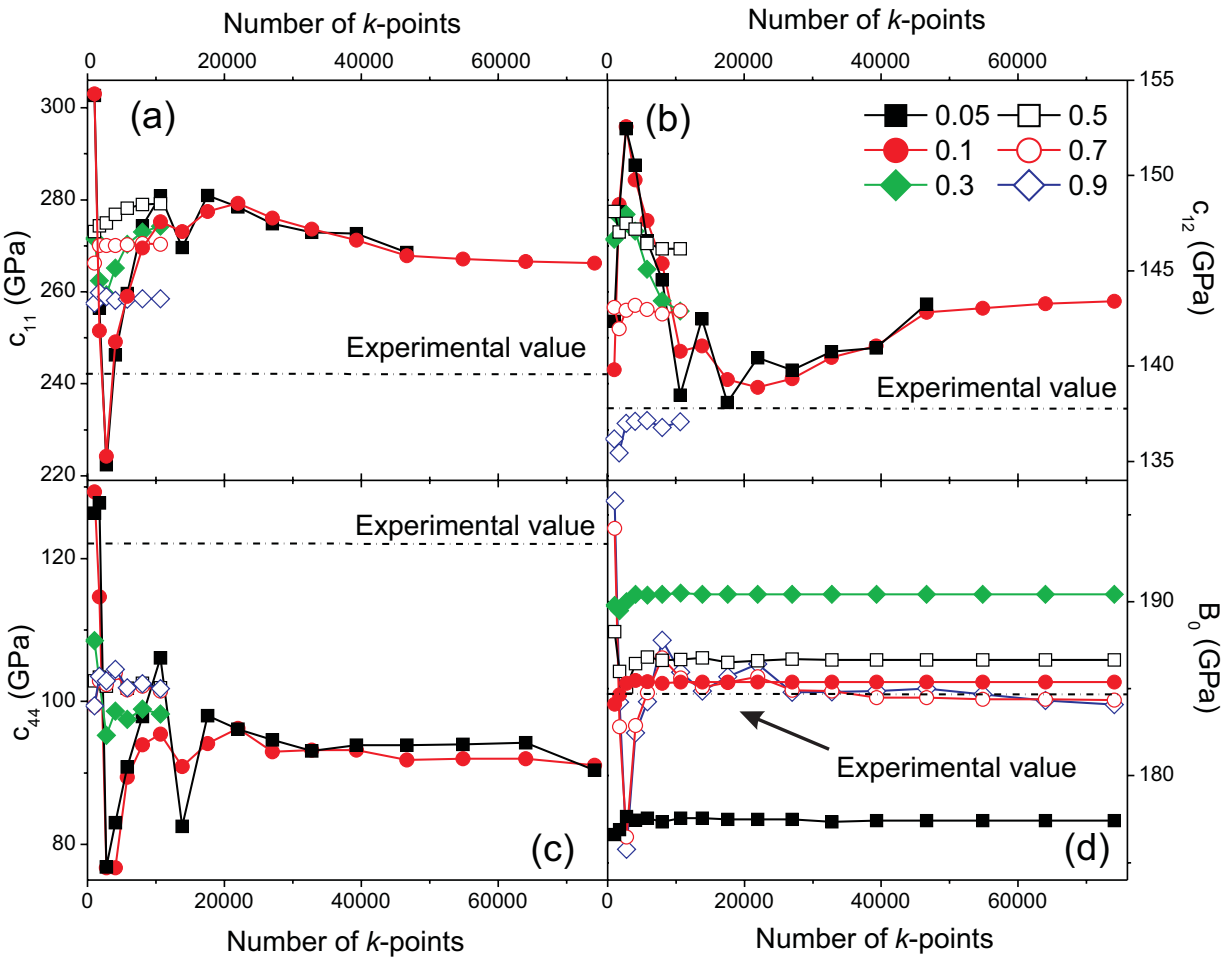

Fig. 1. Calculated dependences of single-crystalline elastic constants of body-centered cubic ferromagnetic Fe as a function of the number of reciprocal-space k-points used to sample the Brillouin zone. The trends were calculated for every elastic constant for a set of six different values of the smearing parameter (from 0.05 eV to 0.9 eV) of the Methfesel-Paxton smearing scheme and are visualized by different symbols.

fig. 1(d)) or systematically overestimating (figs. 1(a),(b)) or underestimating (fig. 1(c)) materials properties. Both the matching and mismatching of experimental values were found in the same materials system, here the bcc ferromagnetic Fe. The systematic underestimation or overestimation visualized in figs. 1(a),(b),(d) also demonstrates that an ideal agreement between theoretical calculations and experimental findings may sometimes not be reached even for the highest values of the convergence parameters (that imply computationally very demanding calculations) due to the errors from the first class mentioned above.

A third class of errors, which shall actually be in the focus of the present paper, is related to the physical *model* that is used to mimic a real materials system in computer simulations. In particular, these errors originate from i) the choice of actual atomistic supercell representing the studied substance, ii) frequent post-processing or analysis of "raw" *ab initio* calculated data that is necessary in order to determine an indirect property of interest, and lastly iii) interfaces between different methods when the calculated and post-processed data are methodologically transferred from one approach to another. In the following, these types of errors will be respectively called *substantial*, *post-processing*, and *multi-methodological* errors.

An illustrative example of a *substantial* error related to the type of computational cell is the modeling of disordered alloys that do not possess any long-range periodicity in the distribution of different chemical elements over the lattice sites. The computational cell modeling such system may not be infinitely large, but needs to be approximated by a smaller cell that is computationally feasible. A suitable computational cell should then not only have a concentration of all chemical species as close as possible to the studied ones, but a special attention should be devoted to the way the atoms are distributed inside. The reliability of the theoretical modeling sensitively depends on, *e.g.*, the type of this atomic distribution and an inconvenient choice may give rise to rather significant errors due to the fact that the distribution of atoms is in reality closely reflecting the chemical properties of alloy constituents.

The *post-processing* errors could be neatly exemplified by the way different collective excitations are taken into account. Thermodynamic properties of materials that depend on, *e.g.*, thermal vibrations can be obtained either from lengthy and computer time demanding molecular dynamic (MD) simulations (with an analysis containing statistical averaging of MD runs necessarily included) or from a clever combination of less exhausting quantum-mechanical calculations of static configurations of atoms and the application of methods of thermodynamics and statistical physics, such as the quasiharmonic approximation (see the next section).

The *multi-methodological* errors occurring when transferring the results from one method to another stem from the fact that the vast majority of industrially interesting/important properties and processes are those that manifest themselves at the macro-scale, but a full electronic-structure or atomistic treatment of macroscopic samples and phenomena is not only impossible, but also meaningless. Therefore, a suitable multi-methodological approach contains a simplified approximative modeling scheme that typically defines i) the realization of abstract entities representing the studied material system in computer within different methodologies, ii) their mutual interactions, and iii) the type of problem-relevant parameters and their scale transfer. The entities replacing theoretically a real system could be subatomic, (*e.g.*, the electronic structure), atomistic, or continuous. Their interactions consequently belong to either quantum mechanics, classical mechanics, or phenomenological theories. The parameter transfer between different descriptions is currently very actively studied as it is often specific to every pair of methods interfacing within the employed multi-methodological scheme. These schemes can be classified, *e.g.*, according to the domain they are intended to bridge, *i.e.* different length or time scales as well as possible hierarchical complexity that is accompanying the scale changes.

As it would be very difficult to provide a comprehensive and exhausting overview of all above described aspects, the present article in its first part illustrates a few selected examples of the above-listed issues. As far as quantum-mechanics–based approaches are concerned, calculations of thermodynamic and elastic properties of materials will be addressed. The former topic is chosen due to both its fundamental importance for nearly any other materials property and its relative scale independence, and the latter was selected in order to exemplify scale-dependent and microstructure-sensitive quantities. The second part then deals with interfaces between quantum-mechanical and atomistic methods on the one side and selected continuum methods on the other side, in particular finite-element method (FEM) simulations, the recently developed fast Fourier transform (FFT) method, and phase-field (PF) simulations.

3 Ab initio approaches to the thermodynamics of materials

3.1 Concepts

As indicated above, established *ab initio* methods are focused on material properties at $T = 0\,\mathrm{K}$. This is on the one hand due to the frozen-in atomic degrees of freedom within the Born-Oppenheimer approximation. The remaining electronic degrees of freedom are then considered within DFT, which is in its original form based on a variational principle yielding only for the ground-state exact results. In 1965 the concepts of DFT have been extended such that also finite electronic temperatures can be taken into account [13]. DFT, therefore, provides for weakly correlated materials a straight forward access to the electronic excitation processes, keeping the same level of accuracy as the calculations of the ground state.

In order to describe the energetics of real materials at finite temperatures, *i.e.*, to obtain results for the free energy of a system, it is, however, necessary to go beyond these approaches and to take all relevant excitation processes into account. For most alloys the configurational entropy, related to the fact that atoms will, at finite temperatures, realize various configurations, and not only those with the lowest energy or the largest disorder, has the largest contribution to the free energy. It can, *e.g.*, be captured with cluster variational methods [14,15] or Monte Carlo simulations based on cluster expansions [16–20]. In the latter the *ab initio* results of numerous crystal structures are used to parametrize a Hamiltonian, which mimics all kinds of atomic interactions. The *post-processing* error related to the truncation of the expansion can efficiently be controlled in cross-validation schemes, making the approach very promising for an *ab initio* derivation of phase diagrams, which are driven by configurational entropy [21].

For pure and ordered systems the entropy due to lattice vibrations has usually the largest impact on the free energy of the involved phases. In principle, the motion of atoms can be considered in a classically exact manner by *ab initio* molecular dynamics simulations. The complete sampling of the phase space is for practical applications, however, computationally too demanding. Therefore, an established method to treat this entropy contribution is the quasiharmonic approximation. Both methods have in common that atomic forces need to be known with high accuracy. Frozen phonon calculations or the derivation of forces from a total energy surface is usually insufficient (*implementation error*), but the applicability of the Hellmann-Feynman [23–25] theorem is decisive. It must be clearly stated that, from this point of view, not all *ab initio* codes are suited for a thermodynamic description of materials.

Within the quasiharmonic approximation the forces entering the dynamical matrix are determined either directly in a supercell approach or perturbatively in reciprocal space using linear response theory. Both approaches have their advantages/disadvantages and a general statement on which of them should be preferred is not possible. For some

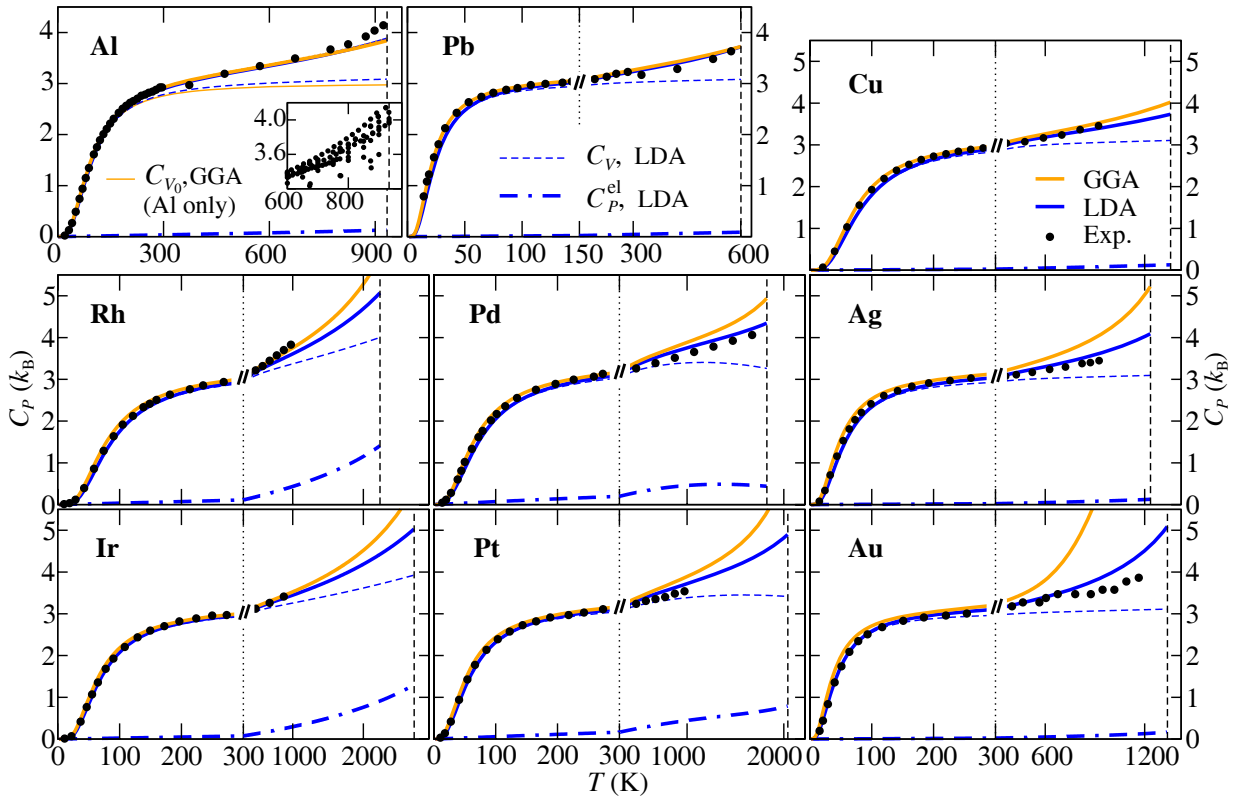

Fig. 2. Isobaric heat capacity C_P as a function of temperature T for a variety of fcc metals, as obtained from a quasiharmonic approximation using only DFT results as input. The contribution due to electronic excitation is also included. The results are obtained at $P = 0$ Pa and are provided in units of the Boltzmann constant k_B. The temperature axis is split by the vertical dotted line into two parts to allow a convenient representation and the melting temperature is indicated for each element by the vertical dashed line. The experimental data are taken from ref. [22].

ab initio codes, however, the choice is narrowed down by the missing implementation of linear response. Within the direct force constant approach great care needs to be taken that a sufficiently large supercell is used to avoid spurious interactions of displaced atoms and to ensure a high sampling of the Brillouin zone in the description of the phonon spectrum. Furthermore, careful convergence tests in particular of the k-point sampling during the electronic integration and the augmentation mesh size in PAW [26] methods have to be performed, to avoid *numerical errors*. A detailed discussion of these errors can for example be found in ref. [27].

Having obtained the phonon excitation energies, thermodynamic potentials like the Helmholtz free energy become directly accessible using statistical concepts (*post-processing*). Free energies are particularly important to make *ab initio* predictions of phase stabilities and phase transformations. This is also the goal of the CALPHAD approach [28], which uses thermodynamic data based on calorimetric measurements. Our recent calculations (see, *e.g.*, [29,30]) do not only show a very good agreement with CALPHAD free energies, with errors of a few meV up to the melting point of some pure, non-magnetic materials. Moreover, it was possible in several cases to provide accurate *ab initio* predictions, where experimental data show large error bars or are, *e.g.*, for metastable phases, not available at all [29, 30].

In this context, it has turned out that the quality of thermodynamic data obtained from the quasiharmonic approximation can best be assessed in the heat capacity data. On the one hand this quantity is much more sensitive to the various sources of errors than the free energy itself, since it is related to its second derivative. On the other hand, the fact that CALPHAD also uses heat capacities as its basic ingredient allows for a very direct comparison with this phenomenological approach. Therefore, we have shown in fig. 2 the isobaric heat capacity obtained for a large set of unary metals. By visualizing only metals that naturally have a fcc crystal structure and are non-magnetic it is allowed to derive systematic trends in the accuracy, which will be discussed in the next subsection.

3.2 Predictive power of ab initio based approaches

Looking at fig. 2, a remarkable agreement of the *ab initio* computed and the available experimental values up to room temperature is observed. The results are almost independent of the chosen exchange-correlation functional (the

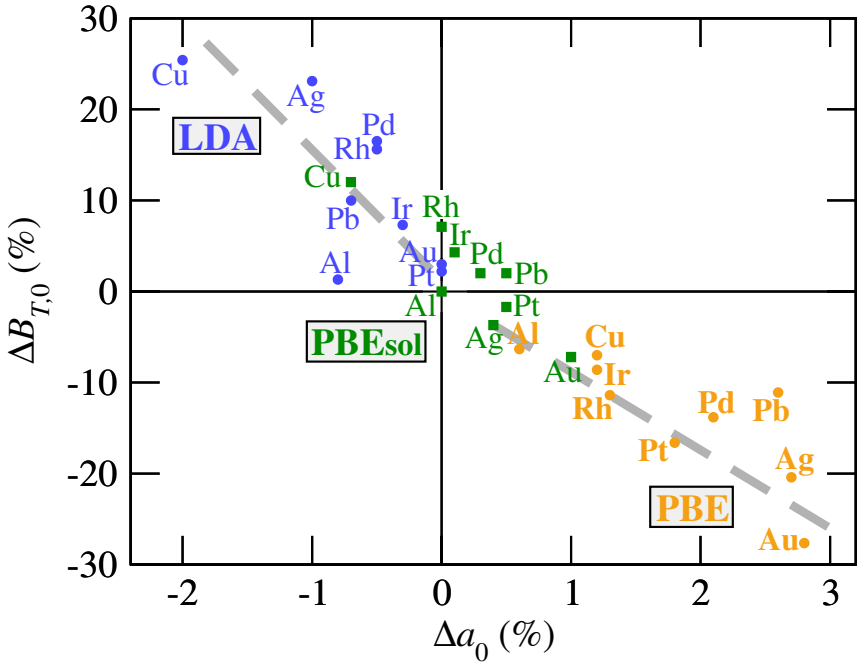

Fig. 3. Correlation between the deviation from experiment for the lattice constants Δa_0 and the bulk moduli ΔB_0. The results for the free different exchange-correlation functionals LDA, PBE, and PBEsol are shown in blue, orange, and green, respectively.

local density approximation (LDA) or the generalized gradient approximation (GGA)), indicating that *methodological errors* are not very decisive in this case. This result is surprising since already at $T = 0\,\mathrm{K}$ the xc-functionals LDA and GGA show noticeable deviations in fundamental properties like the lattice constant and the bulk modulus.

As can be seen in fig. 3 the LDA systematically underestimates the lattice constant for the investigated metals, reflecting the well-known overbinding inherent to this approach. At the same time the bulk modulus of the metals is overestimated by the LDA. The errors of the $T = 0\,\mathrm{K}$ material properties can be very small, as, *e.g.*, for Au or Pt, but can also reach up to 2% for the lattice constant and 25% for the bulk modulus, as, *e.g.*, for Cu. Nevertheless, the errors in the heat capacity of the involved materials seem even in the region where they become noticeable at a first glance only weakly related to the accuracy of the ground-state properties.

From the available GGA functionals, we have focused in fig. 3 on the PBE [31] version. This functional yields for all studied elements a lattice constant that is larger and a bulk modulus that is lower than the experimental values, respectively. At the same time we observe in the heat capacity data of fig. 2 that PBE always yields higher values than LDA. This becomes particularly relevant close to the melting point (dashed vertical lines in fig. 2) and in many cases the agreement of LDA with experimental data above room temperature seems to be better than the one of GGA. Still, a general statement, in which xc-functional should be preferred, is not possible. Instead, it seems to be justified to use the *methodological error* as an indication for the predictive power of this approach: A small deviation between the different theoretical data indicates that a very good agreement with experimental data can be expected. If, however, the theoretical results depend very much on the choice of the xc-functional then the predictive power of the *ab initio* approach is rather poor.

With PBEsol [32] fig. 3 also contains data for the lattice constant and the bulk modulus of another xc-functional. Due to the construction of this functional, these data show a much better agreement with experiment than the previous two functionals. Instead of using this functional, we even went one step further and directly took the experimental values for the lattice constant and the bulk modulus as an input for our thermodynamic calculations. The results of this mixed approach of theory and experiment are shown in fig. 4. We observe, first of all, that the situation of GGA and LDA has been exchanged, now. In contrast to fig. 2, it is now the LDA approach, which always yields the higher value for the heat capacity and the GGA, which generally shows the better agreement with experiment. Nevertheless, the statement of the predictive power, depending on the relative difference between the *ab initio* approaches, remains valid.

Remarkable is the much better agreement of the mixed approach for both LDA and GGA, with the experimental values as compared to complete *ab initio* calculations. This indicates that the *methodological errors* we introduce by approximating the exchange-correlation functional are much more significant for the $T = 0\,\mathrm{K}$ data than possible *post-processing errors* from the thermodynamic description.

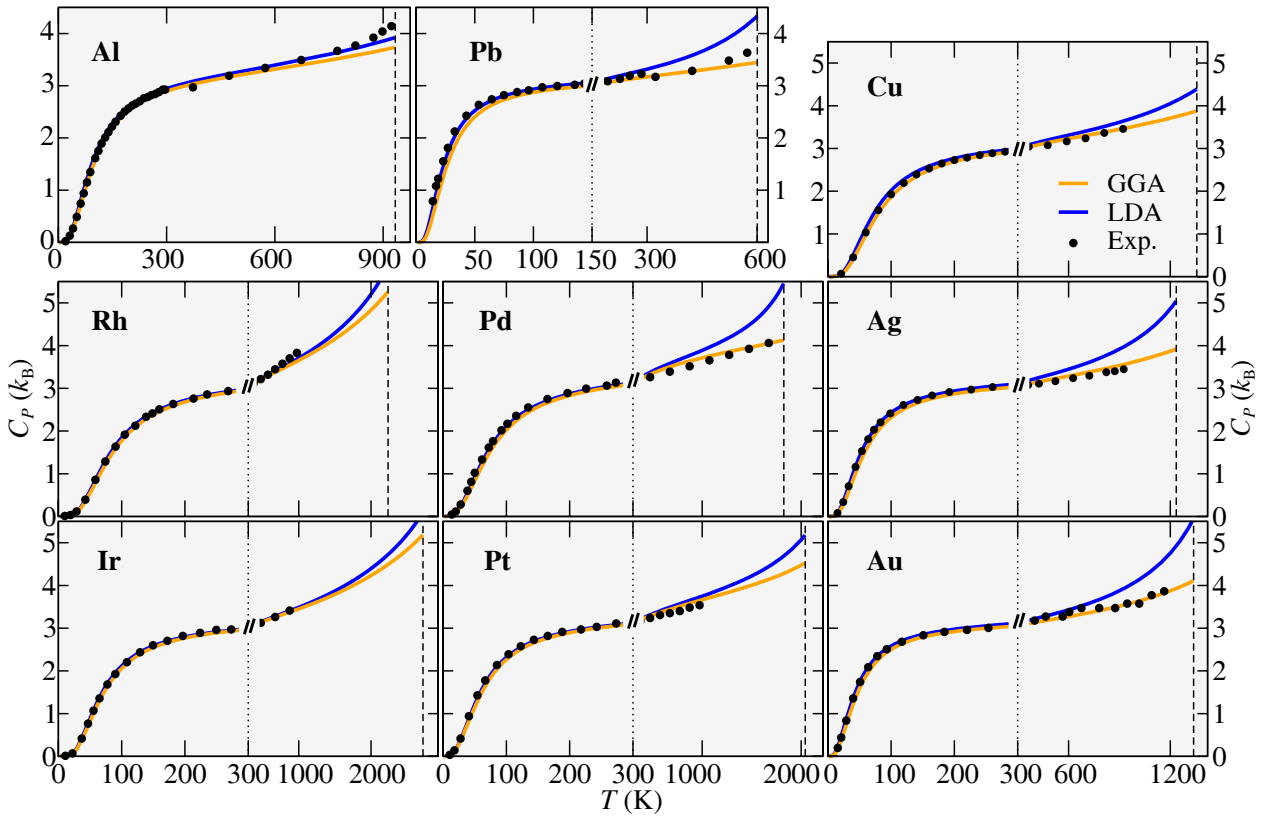

Fig. 4. Same as fig. 2, but with a mixed approach for the input at $T = 0\,\mathrm{K}$. Here, the method is not solely *ab initio*, since the values for the lattice constant and the bulk moldulus are taken from experiment, whereas the complete temperature dependence is only obtained from *ab initio* calculations.

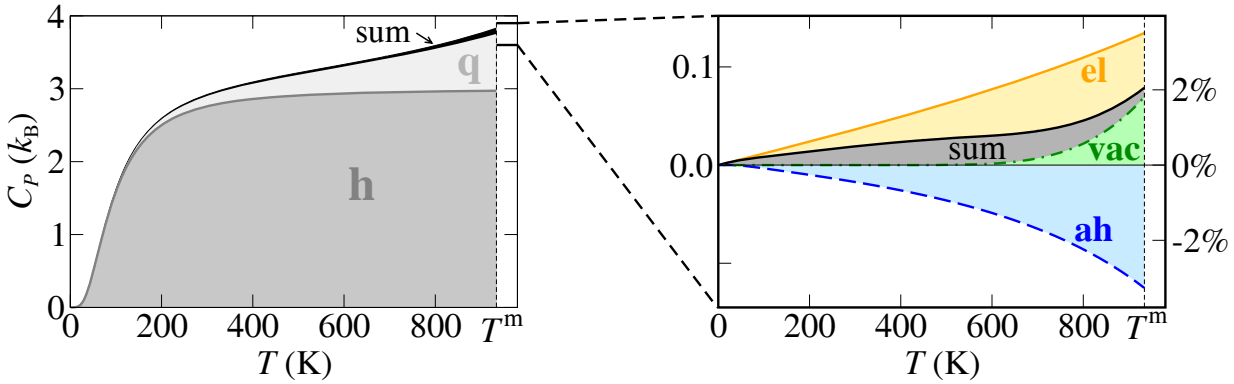

Fig. 5. Isobaric heat capacity for aluminium. The figure shows the influence of various corrections to the quasiharmonic approximation.

For some elements, such as Al, noticeable deviations between theory and experiment are observed (in particular close to the melting point), whereas the two tested xc-functionals show almost perfect agreement. This seems to be in contrast with the statement on the predictive power of our thermodynamic approach, mentioned previously. However, the reason for this behaviour can be resolved by pointing out the *post-processing error* when focusing on the quasi harmonic approximation as the only excitation process determining the entropy. The remaining deviations between theory and experiment actually indicate that further excitation processes need to be considered, which have not been taken into account so far. Figure 5 indicates which further processes are, *e.g.*, relevant in Al. The detailed analysis [29] actually solves a long-standing debate if the presence of vacancies or the contribution of explicit anharmonicities (beyond the quasiharmonic approximation) explains the exponential increase of the heat capacity of Al close to the melting point. As can be seen in fig. 5, the vacancies are observed to provide the correct qualitative behaviour. Taking

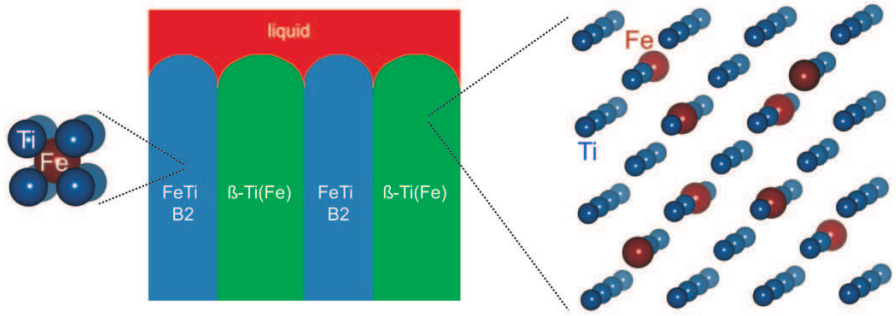

Fig. 6. Schematic visualization of two computational unit cells representing phases solidifying in eutectic Fe-Ti system, namely the one for the ordered FeTi intermetallics with the B2 (CsCl) structure on the left and the supercell with the minimum number of the Fe-Fe pairs as a model for the β-Ti(Fe) on the right.

all relevant contributions into account, the overall deviation between both functionals is again very small, as confirmed by the comparison with experiments, and yields a very high predictive power.

4 Quantum-mechanical approaches to the elasticity of materials

Theoretical multi-scale approaches combining i) *ab initio* calculations and ii) linear-elasticity and/or continuum methods became increasingly popular (see, *e.g.*, [33–36]) to predict the elastic response of polycrystals on the macroscopic scale. Using i) quantum-mechanical thermodynamic stability data and single-crystalline elastic properties of different phases with ii) microstructure-specific homogenization methods in order to predict macroscopic experimentally detectable elastic parameters of new materials has become a modern alternative to classical metallurgical concepts. This so-called theory-guided materials design (TGMD) represents a scale-bridging scheme that is directly linking the atomistic and macroscopic levels and allows i) systematic scanning of numerous chemical compositions via high-throughput quantum-mechanical calculations and thus ii) pre-selection of the most promising materials candidates. Consequently, a significant reduction of experimental costs and time is achieved when designing new materials with application-determined properties.

The TGMD strategy has been recently successfully applied in developing biocompatible Ti-based implant materials with bone-matching elastic properties [37,38]. Another example when this scheme proved to be successful was the search for Mg-Li binaries and MgLi-based ternaries optimized with respect to multiple partly conflicting criteria, specifically the density, stiffness, and ductility [39–43]. The research resulted in a quantitative description of fundamental materials design limitations that prevent single-phase materials from having both high stiffness and high ductility.

The same concepts can be applied also to existing multi-component materials with complex microstructures in order to shed more light on the structure-property/components-property paradigm and deepen our understanding of the fundamental mechanisms responsible for macroscopic materials behavior that often have their origin at the atomic scale. In this spirit, multi-scale hierarchical biocomposites as, *e.g.*, a lobster cuticles have been modeled and allowed to study and analyze nature's evolutionary designing approaches resulting in extremal properties [44–48].

Below, the combination of *ab initio* computed single-crystalline elastic tensor with different homogenization methods will be illustrated for a few selected examples. First, an example of *substational* errors frequently occurring in the quantum-mechanical calculations will be discussed in subsect. 4.1. Then, the methodology of single-crystalline constants calculations will be summarized (sect. 4.2) followed by classical linear-elasticity homogenization schemes applied to determine integral elastic response of polycrystalline aggregates (sect. 4.3). Lastly, the mathematical backbone of these multi-scale homogenization schemes will be discussed in order to analyze their error-propagation properties (sect. 4.4).

4.1 Substantial errors in ab initio calculations

Substantial errors related to the computational cell may be nicely exemplified on one of two phases that appear during the solidification of eutectic Fe-Ti alloys (see fig. 6). The ordered FeTi intermetallics with 50 at% of both components and the B2 structure (CsCl) easily comply with the periodic boundary conditions implemented in most of solid-state computational packages. The corresponding unit cell representing a defect-free FeTi phase contains only 2 atoms. In contrast, the experimentally disordered β-Ti(Fe) phase lacks any long-range periodicity and due to its concentration,

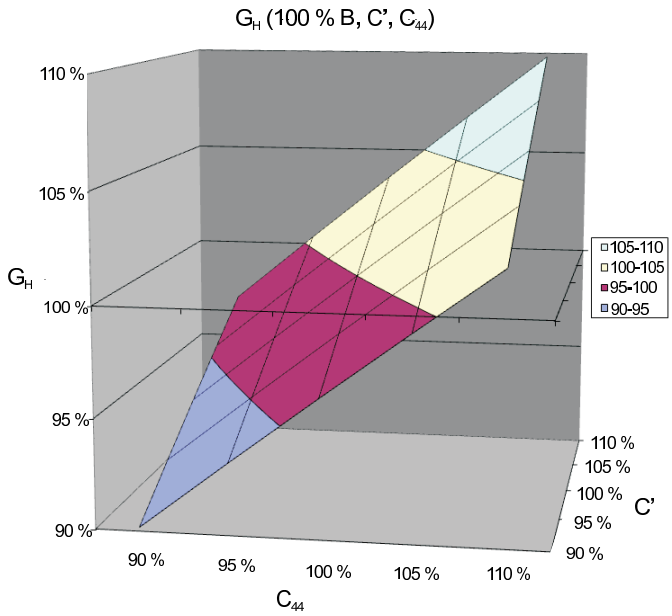

Fig. 7. The induced changes of the polycrystalline shear modulus G_{H} calculated employing the Hershey homogenization scheme as a function of the changes of the *ab initio* calculated elastic tensor components C' and C_{44} with the bulk modulus B kept constant (for details see [12]).

Table 1. For four 54-atomic supercells of $Ti_{46}Fe_8$ including the structure in fig. 6 and three different special quasi-random (SQS) supercells (SQS1, SQS2, SQS3), the numbers of the first nearest Fe-Fe pair (N1) and the second nearest Fe-Fe pair (N2), and the formation energy per atom E_f (meV) are given.

	N1	N2	E_f (meV)
SQS1	0	2	−79.6
SQS2	0	3	−67.2
SQS3	2	3	−41.4
supercell in fig. 6	0	0	−83.0

85 at% Ti, that may not be expressed as a ratio of small natural numbers, the size of the cell, its shape, as well as the actual distribution of atoms must be carefully chosen.

As far as the size is concerned, a 54-atomic supercell with a 8/46 ratio of Fe and Ti atoms inside allows for modeling of 85.185 at% Ti, very close to the experimentally observed value of 85 at% Ti. To compute single-crystalline elastic constants it is advantageous to use such a shape that has the symmetry of the underlying crystalline lattice (see, *e.g.*, our recent paper [49] for details). Due to the fact that the atoms in the β-Ti(Fe) phase are distributed over body-centered cubic lattice sites, the cubic shape of the supercell was chosen (see right-hand side of fig. 6). Lastly, when looking for the best distribution of atoms inside of the β-Ti(Fe) supercell, the fact that the experimental alloys do not possess any long-range periodicity should be taken into account as well as the individual chemical interactions between both chemical species in the studied binary system. As far as the latter aspect is concerned, our formation-energy analysis revealed unexpected repulsive short-range interactions between pairs of either Fe or Ti atoms and lead to a depletion of atoms of the same kind from the first atomic coordination shells. This depletion effectively leads to a reduced disorder, or equivalently partial ordering tendencies, in the Fe-Ti alloys. The fact that the depletion of Fe and Ti atoms of the same kind is rather inherent to the whole binary system (independently of the actual concentration) can be easily exemplified in case of the other phase, FeTi B2 intermetallics (see left-hand side of fig. 6), in case of which, *e.g.*, every Fe atom is surrounded by eight Ti atoms (see examples from other systems, *e.g.*, in [50–52]).

In order to quantitatively analyze the depletion a series of so-called special quasi-random (SQS) supercells (see, *e.g.*, [53–61]) were constructed with the local atomic arrangements restricted so as to not contain atoms of the same kind occupying the neighboring atomic shells. The results obtained for these restricted supercells are summarized in table 1 containing both the number of Fe-Fe pairs and the corresponding formation energy. This is compared with the values of the supercell, shown in fig. 6, designed to have the minimum amount of the Fe-Fe pairs and possess the cubic symmetry. This supercell was calculated to have the lowest energy out of the studied set of supercells.

Taking into account the Fe distribution in the Ti matrix, the interactions of the first nearest neighbor Fe-Fe pairs and the second nearest neighbor Fe-Fe pairs are found to play a decisive role in the structure stability. As shown in table 1, the fewer such Fe-Fe pairs are in the structure, the lower the formation energy and thus the more stable the structure. Due to the super-cell size constrains, the maximum reduction of the Fe-Fe pairs was achieved in a supercell, where only two second-nearest-neighbor Fe-Fe pairs are present. As can be seen in table 1 the formation energy is still about 3.4 meV per atom higher than the energy of the supercell shown in fig. 6. The supercell modeling the β-Ti(Fe) phase thus nicely illustrates the importance of detailed thermodynamic analysis preceding any elasticity study (see also, *e.g.*, [62–64]). Therefore, specifically in case of disordered alloys, a state-of-the-art approach would be to perform a full cluster-expansion analysis of thermodynamic properties (see, *e.g.*, [65]) prior to cluster-expanding elastic properties (see for example [66]).

4.2 Ab initio prediction of single-crystalline elastic properties

When the computational supercell representing the system is properly set, single-crystal elastic constants C_{ij} can nowadays be routinely predicted from *ab initio* calculations. For this purpose, the total energy changes are calculated as a function of specific lattice distortions applied to the undistorted ground state (see, *e.g.*, Cheng *et al.* [67]). For a cubic crystal three elastic constants are needed, *i.e.* three different distortions have to be studied. The first distortion is the isotropic volume expansion or compression, *i.e.* the energy-volume dependence. The second derivative at the minimum of the energy-volume curve determines the bulk modulus B_0 employing, *e.g.*, the Murnaghan equation of state [68]. The bulk modulus can also be expressed as a linear combination of two elastic constants:

$$V\left(\frac{\partial^2 E}{\partial V^2}\right)_{V_{\mathrm{eq}}} = \frac{1}{3}(C_{11}+2C_{12}) = B_0. \tag{1}$$

The other two deformations ϵ along the [001] and [111] directions may be expressed by the following strain tensors:

$$\epsilon^{[001]} = \begin{pmatrix} -\delta/2 & 0 & 0 \\ 0 & -\delta/2 & 0 \\ 0 & 0 & \delta \end{pmatrix}, \qquad \epsilon^{[111]} = \begin{pmatrix} 0 & \delta & 0 \\ \delta & 0 & 0 \\ 0 & 0 & 0 \end{pmatrix}. \tag{2}$$

Here, δ is the distortion determining the lattice distortion and is limited in this study to ± 0.05 in order to avoid non-linearities in the total energy dependence. The corresponding changes of the total energy $E(\epsilon)$ with respect to the energy of the ground state E_0 are then divided by the volume V in order to calculate the elastic energy density $U^{\epsilon} = (E(\epsilon) - E_0)/V$ that is linked for each kind of distortion to specific elastic constants as

$$\frac{\partial^2 U^{[001]}}{\partial \delta^2} = \frac{3}{2}(C_{11}-C_{12}) = 3C', \tag{3}$$

$$\frac{\partial^2 U^{[111]}}{\partial \delta^2} = 4C_{44}. \tag{4}$$

Using these relations, all elastic constants can be obtained by standard total energy calculations.

4.3 Linear-elasticity approaches to polycrystalline elastic response

In order to translate the elastic constants of a single crystal to that of a realistic engineering material, which is a polycrystal, various homogenization approaches have been proposed in the past. The *Voigt scheme* assumes that the local strain is equal in all the grains of a polycrystal, *i.e.* the strain compatibility condition is satisfied. However, this approach assumes a stress discontinuity across the grain boundaries. The strain compatibility assumption leads to a polycrystalline bulk modulus B_{V} and a shear modulus G_{V}

$$B_{\mathrm{V}} = B_0 = \frac{1}{3}\left(C_{11}+2C_{12}\right), \tag{5}$$

$$G_{\mathrm{V}} = \frac{C_{11}-C_{12}+3C_{44}}{5} = \frac{2C'+3C_{44}}{5}. \tag{6}$$

The *Reuss homogenization* is based on a constant local stress assumption, *i.e.* it satisfies the mechanical equilibrium conditions, but requires a geometrical misfit between adjacent grains. The assumption of constant stress leads to a polycrystalline shear modulus G_{R} that is expressed as a function of elastic compliances S_{ij}:

$$G_{\mathrm{R}} = \frac{5}{4(S_{11}-S_{12})+3S_{44}} \tag{7}$$

where the relationship between S_{ij} and C_{ij} for materials with cubic symmetry is

$$S_{11} = \frac{C_{11} + C_{12}}{(C_{11} - C_{12})(C_{11} + 2C_{12})}\,, \tag{8}$$

$$S_{12} = \frac{-C_{12}}{(C_{11} - C_{12})(C_{11} + 2C_{12})}\,, \tag{9}$$

$$S_{44} = \frac{1}{C_{44}}\,. \tag{10}$$

Equation (7) can be re-written in terms of C_{ij} as

$$G_{\mathrm{R}} = \frac{5(C_{11} - C_{12})C_{44}}{4C_{44} + 3(C_{11} - C_{12})} = \frac{10C'C_{44}}{4C_{44} + 6C'}\,. \tag{11}$$

For the *Hershey method*, the homogenized polycrystalline shear modulus G_{H} is given as a root of a polynomial and there are two different expressions available in the literature. The original paper by Hershey [69] gives the following quartic equation:

$$\begin{aligned} &64G_{\mathrm{H}}^4 + 16(4C_{11} + 5C_{12})G_{\mathrm{H}}^3 + [3(C_{11} + 2C_{12})(5C_{11} + 4C_{12}) - 8(7C_{11} - 4C_{12})C_{44}]G_{\mathrm{H}}^2 \\ &- (29C_{11} - 20C_{12})(C_{11} + 2C_{12})C_{44}G_{\mathrm{H}} - 3(C_{11} + 2C_{12})^2(C_{11} - C_{12})C_{44} = 0. \end{aligned} \tag{12}$$

This 4th-order polynomial is used in the majority of recently published papers [33–35]. In contrast, the paper by Tang *et al.* [36] refers to the 3rd-order polynomial

$$G_{\mathrm{H}}^3 + \frac{1}{8}(5C_{11} + 4C_{12})G_{\mathrm{H}}^2 - \frac{1}{8}C_{44}(7C_{11} - 4C_{12})G_{\mathrm{H}} - \frac{1}{8}C_{44}(C_{11} - C_{12})(C_{11} + 2C_{12}) = 0 \tag{13}$$

originally proposed by Ledbetter [70].

For systems fulfilling the conditions of mechanical stability: $B > 0$, $C_{44} > 0$, $C' > 0$ both eqs. (12) and (13) change the sign of their coefficients only once and therefore have only one real-valued root for a given set of elastic constants. This single root is identical in eqs. (12) and (13).

Another mathematically very simple method has been proposed by Hill [71] and Gilvarry [72]. This is the *Reuss-Voigt-Hill-Gilvarry* (RVHG) method according to which the polycrystalline modulus is assumed to be the arithmetic mean of the Reuss and Voigt extremes:

$$G_{\mathrm{RVHG}} = \frac{1}{2}\left(G_{\mathrm{R}} + G_{\mathrm{V}}\right). \tag{14}$$

The bulk modulus B for systems with cubic symmetry as considered here has the same expression, eq. (1), in all four methods, and $B_{\mathrm{V}} = B_{\mathrm{R}} = B_{\mathrm{H}} = B_{\mathrm{RVHG}}$.

Once the homogenized elastic constants are known, other elastic constants, such as the Young's modulus Y or Poisson's ratio ν, can be easily obtained:

$$Y = \frac{9B_0G}{3B_0 + G}\,, \qquad \nu = \frac{1}{2}\frac{3B_0 - 2G}{3B_0 + 2G}\,. \tag{15}$$

Here, G is equal to G_{V}, G_{R}, or G_{H}.

4.4 Error propagation properties of analytical multi-scale elasticity schemes

An important issue which has been studied only recently in case of theoretical multi-scale approaches combining i) *ab initio* calculated single-crystal elastic constants and ii) linear-elasticity continuum methods is that practical multi-scale approaches do not rely on absolutely accurate quantities even at the finest scale [73]. For example density functional theory which is often used at the finest level cannot be systematically improved by eliminating residual errors (see above) but is limited by systematic errors such as the availability/choice of the exchange-correlation functionals. Therefore, a crucial aspect to employ multi-scale strategies is a careful analysis of how these intrinsic errors propagate from the finest and most fundamental scale/level to the applicationally relevant level on the coarsest scale.

The sensitivity with respect to error propagation of four commonly employed multi-scale approaches, which have been developed to predict to the integral elasticity of non-textured polycrystals with cubic symmetry, namely that of Voigt [74], Reuss [75], Voigt-Reuss-Hill-Gilvarry (VRHG) [71,72], and Hershey [69], have been studied recently [12].

The four studied methods have different underlying models based on different assumptions and range from mathematically simple ones, as, *e.g.*, those of Reuss, Voigt and their average (Voigt-Reuss-Hill-Gilvarry), to more complex self-consistent schemes as that of Hershey. All four examined multi-scale methods scale-transfer the single-crystal elastic constants employing a mathematical backbone that may be analyzed with respect to its error propagation properties. The sensitivity of the final homogenized polycrystalline shear modulus G was analyzed by Friák *et al.* [12] i) analytically for the partial derivatives of G with respect to the individual elastic constants (in case of Voigt and Reuss schemes), and ii) numerically for all four schemes.

The main conclusion of the study was that the sensitivity of Hershey and VHRG shear moduli with respect to the input single-crystalline elastic constants B, C', C_{44} is nearly linear (see fig. 7) and lies within the limits found for the Voigt and Reuss schemes for a broad set of materials with very different physical properties. The influence of the bulk modulus was found to be approximately two orders of magnitude smaller than that of C' and C_{44} and our results show a strong sensitivity with respect to the elastic anisotropy. In particular the self-consistent Hershey scheme was found to behave very similarly to the averaging VRHG scheme in both absolute values of the homogenized shear modulus and error propagation properties.

5 Interfaces between ab initio and continuum methods

A main drawback of the homogenization approaches mentioned above is that they give accurate predictions of the average properties of materials structure but are unable to capture the local development of the stress and strain fields within each point of the material. Therefore the detailed simulation of such important large-strain phenomena like damage initiation, energy dissipation and failure strength is not possible. One way to deal with this problem is to use the classical finite-element method (FEM). However, in the case when many hierarchy levels are required, this approach becomes computationally inefficient. The fast Fourier transforms (FFT) method emerges as a promising, computationally less expensive alternative. After discussing a few selected examples of multi-methodological combinations of *ab initio* results with both FEM (sect. 5.1) and FFT (sect. 5.2) methods, this section will be closed with a discussion of challenges at the interface between quantum-mechanical and atomistic methods on one side and phase-field modeling on the other (sect. 5.4).

5.1 Ab initio calculations interfacing finite-element methods

Crystal-based finite-element methods (FEM) are versatile continuum approaches for predicting mechanical properties and deformation-induced crystallographic textures. They can be applied to both elastic-plastic and elastic problems. The methodology is based on i) a detailed understanding of the underlying crystal deformation mechanisms and ii) a number of constitutive material parameters that are often difficult to measure. First-principles calculations, that take into account the discrete nature of matter at the atomic scale, are an alternative way to study mechanical properties of single crystals without using empirical parameters.

In our recent study [38] we demonstrated how to combine these two well-established modeling tools, *ab initio* modeling and crystal mechanical FEM, for an improved approach to design polycrystalline materials. The starting point is the use of quantum-mechanical predictions based on density functional theory. The results of the DFT calculations [1,2], namely the elastic constants and the chemical composition, are subsequently up-scale transferred in crystal-based finite element simulations. The latter method comprises a group of continuum-based approaches which consider the tensorial nature of elastic-plastic crystalline deformations and the orientation distribution in a (poly-) crystalline aggregate. In the case of purely elastic problems, the method is referred to as crystal elasticity finite element method (CEFEM) and in the case of elastic-plastic loading it is referred to as crystal plasticity finite element method (CPFEM) [76–81]. The crystal plasticity provides a micromechanical model for slip-dominated plastic flow and serves as a constitutive theory. The finite element method offers a numerical means to solve partial differential equations, such as the field equations of elasticity and plasticity. Both of these are combined together in the CPFEM [82]. Crystal plasticity theory stemmed from Taylor's work [83] and a theoretical description may also be found, *e.g.*, in refs. [84,85].

Both methods were applied for the investigation of two engineering problems. The first one is the evolution of the crystallographic texture during elastic-plastic plane strain deformation (idealization for cold rolling) as a function of the magnitude and anisotropy of the elastic stiffness. The second one is the prediction of the overall elastic stiffness of a textured polycrystal in case of reversible bending for different elastic tensors. Both topics represent important problems for the development of physically-based multi-scale models that can be used to predict thermomechanical processes and process-dependent homogenized properties of polycrystalline metals. A more detailed description of the constitutive model is given in [76,86]. The combined methodology was applied to three body-centered cubic (bcc, β) Ti-Nb alloys for biomedical applications as an example since both the crystallographic texture evolution and the texture-dependent elastic stiffness play an essential role for these materials with respect to biomedical applications.

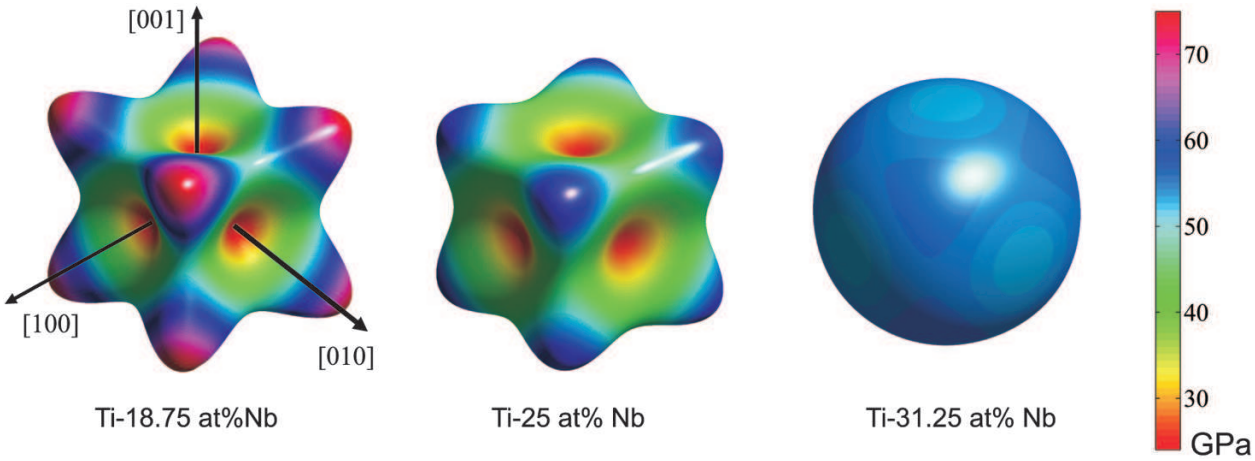

Fig. 8. Young's modulus surface plots of Ti-18.75 at% Nb, Ti-25 at% Nb, and Ti-31.25 at% Nb.

The *ab initio* part of the study (partly published in [37]) focused on the single-crystal cubic elastic constants and revealed a strong compositional dependence of the magnitude and elastic anisotropy (see fig. 8). Ti-18.5 at% Nb reveals the strongest elastic anisotropy. Ti-31.25 at% Nb is nearly isotropic. Demonstrating the performance of our scale-bridging simulation concept that combines first-principles modeling with crystal-based finite element homogenization, these elastic single-crystal tensors obtained by DFT were then used for calculating the overall stiffness for the three polycrystalline alloys employing both the CEFEM and CPFEM methods (see the results summarized in ref. [38]).

The use of a crystal-based finite element method did not only provide a homogenization model for obtaining polycrystal averages of elastic data in the case of a non-random crystallographic orientation distribution but it also allows to study details of grain-to-grain heterogeneity in metals [77–79]. This point is of high relevance since polycrystals as a rule do not deform homogeneously but tend to reveal strain localization and substantial inter- and intra-grain stress-strain inhomogeneity that cannot be captured by analytical approximations. Likewise, the use of *ab initio* predicted elastic tensor data in a CPFEM environment is of high benefit since for many complex metallic alloys the corresponding single-crystal elastic tensor data are not available from experiments. For some metallic materials, particularly if they have a high melting point, complex chemical composition, or reveal phase transformations during cooling from the melt, single crystals cannot be produced. In such cases, *ab initio* simulations are the only way for obtaining the elastic tensor data as input into corresponding finite element simulations.

5.2 Ab initio elasticity interfacing fast Fourier transform method

An alternative approach, to even go beyond the elastic regime and consider elasto-viscoplastic properties at large deformations, is a new fast Fourier transform (FFT) method proposed first by Moulinec and Suquet [87,88] for composite materials and later extended to both elastic and viscoplastic polycrystals by Lebensohn and co-workers, (*e.g.*, [89–95]).

The FFT-based method is suitable to investigate the mechanical response of composite and polycrystalline materials as a function of microstructural parameters such as: volume fraction, size, shape and contiguity of phases in composites, and crystallographic and morphological texture in polycrystals. Essentially, the following steps are taken: i) hypothetical microstructures are generated such that their representativeness can be validated by comparison with the available experimental data; ii) the three-dimensional microstructural parameters of those hypothetical microstructures are measured; and iii) these are used as input for property simulation. Having measured the microstructural parameters from a representative three-dimensional digital microstructure, a property simulation model can be used to evaluate which combination of the microstructural parameters results in the desired mechanical state of the material for a given external load.

In general, the FFT is faster than the FEM, works with arbitrary contrast in the properties of the phases or grains and is particularly suitable for materials with perfect periodicity. Unlike the FEM, the FFT method does not require discrete meshing of the geometry. Instead, a piece of material with microstructure is discretized in equal prismatic pixels, where to each pixel the properties of the respective phase or grain of the real microstructure are assigned. An important advantage of this method is that it can use microstructures obtained from experimentally measured images or from other simulation techniques, like the phase-field model (see sect. 5.4). This FFT-based formulation provides detailed information about the local values of the stresses and strains in the phases or grains at large deformations, and therefore the mechanisms of damage initiation and failure can be obtained.

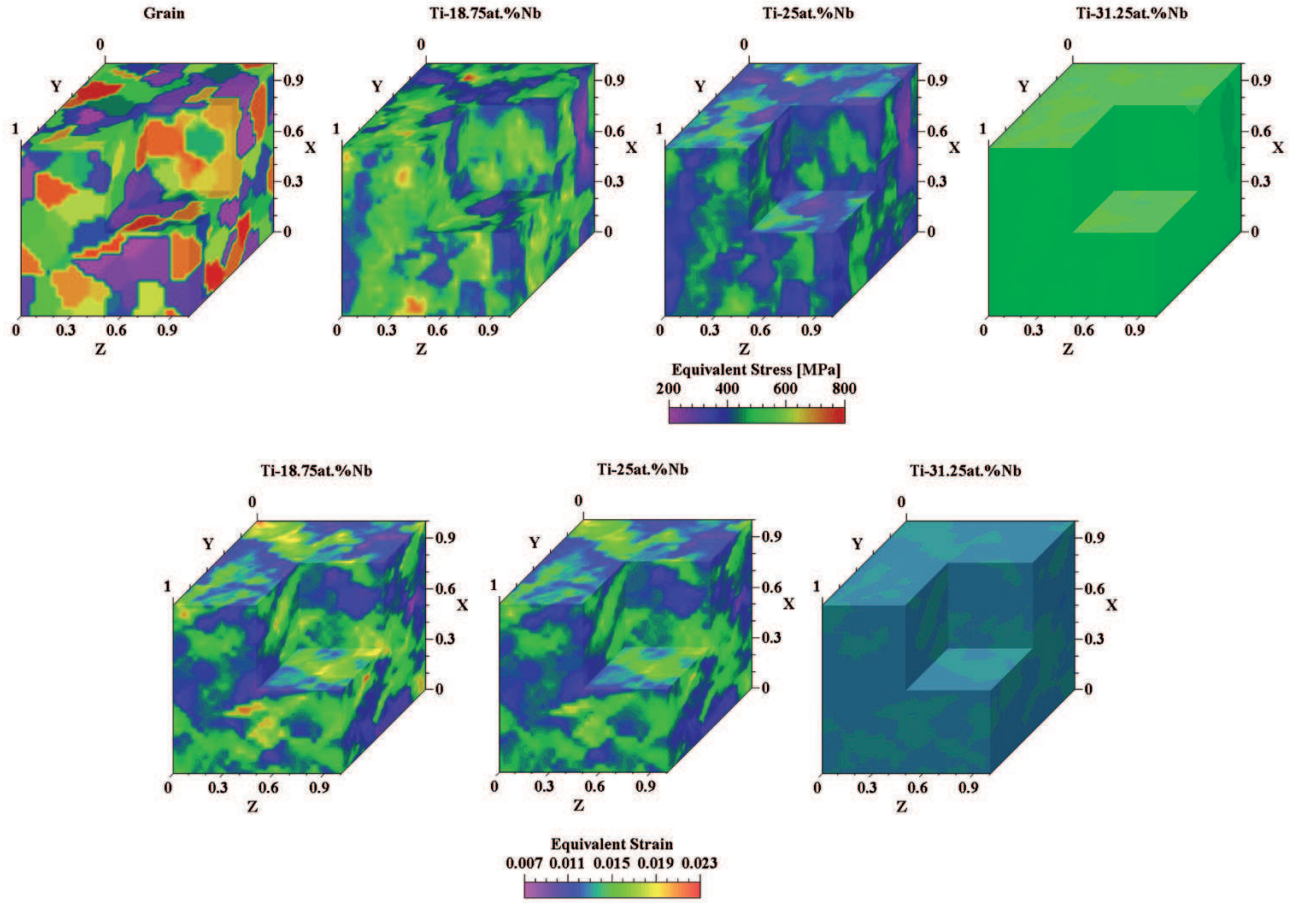

Fig. 9. 3D plots of equivalent stress and equivalent strain distribution throughout the volume obtained from FFT calculation employing *ab initio* determine elasticity parameters of Ti-Nb as visualized in fig. 8.

The capability of the FFT-based method is illustrated in fig. 9. For a model polycrystalline aggregate (the first picture in the upper row in fig. 9), 3D plots of equivalent stress (upper row) and equivalent strain (lower row) distribution throughout the volume of aggregates are shown for the three Ti-Nb alloys mentioned in the previous sect. 5.1. The results were obtained from FFT-based calculations when the elastic tensors were taken in each case from the corresponding *ab initio* calculation (see the first-principles calculated directional dependence of Young's modulus in fig. 8). Due to the fact that the simulated polycrystalline aggregate was identical for all three Ti-Nb alloys, the figures clearly show differences in stress and strain distribution due to different single-crystalline elasticity.

5.3 Computational challenges in electronic-structure and atomistic calculations of grain boundaries

Despite the successfully combined quantum-mechanical and FEM/FFT approaches summarized above, there are a few very challenging aspects in these simulations that have not been yet fully addressed. In particular, theoretical methods dealing with i) grain boundaries (see, *e.g.*, [96–100]) in their full complexity and/or ii) deformations beyond the linear-elasticity regime (see, *e.g.*, [101–121], or [122–133] as well as [134–154]) are still intensively studied in order to seamlessly interface them with continuum methods. Due to the fact that the deformations beyond the linearity regime were discussed in our recent review [155], this subsection will focus on computationally demanding aspects related to grain boundary (GB) properties. GBs constitute a larger and more general class of interfaces in solid state that break the continuation of the lattice plane across the boundary. One of the major challenges that the study of GBs imposes is the number of macroscopic degrees of freedom required to describe and identify a GB: for a complete macroscopic description a five dimensional configurational space is necessary (see, *e.g.*, ref. [156,157] and references therein).

By employing either quantum-mechanical or atomistic simulations, GBs may be modeled by a supercell containing a pair of mutually compensating defects or by a slab or cluster geometry involving a single defect (see details, *e.g.*, in [157]). The use of a self-compensating pair in the supercell geometry is necessary in order to restore the translational

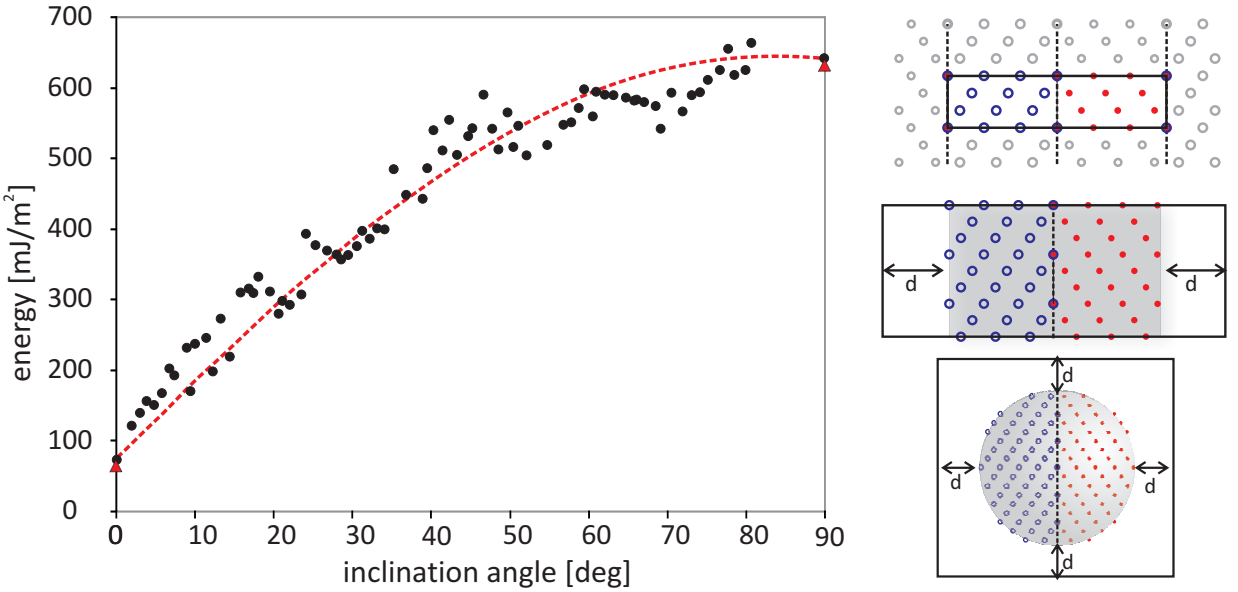

Fig. 10. Computed energies $\Sigma 3$ GBs for various boundary inclination angles (rotations) around the [110] axis. The red (black) triangles (circles) are *ab initio* (MEAM) computed energies, respectively. The GB at 0° (90°) inclination angle corresponds to the $\Sigma 3\{111\}(\{1\text{-}12\})$ GB, respectively. For all the inclination angles the smaller (*i.e.* 1×1) interface reconstruction has been implemented. Right side: Schematic representation of a supercell, slab, and spherical cluster geometry. The dashed lines indicate the position of the interface. d is the vacuum thickness in the slab/cluster geometry, when periodic boundary conditions are used.

symmetry of the system which is destroyed by the presence of a single GB. As far as the slab/cluster geometry is concerned, further complications stem from an *a priory* unknown effect that free surfaces have on the atomic geometry, electronic structure and total energy of the system under consideration. Moreover, different grain boundary misorientations impose different free surfaces. Thus, even the relative comparison of two defects is a puzzling situation. However, both slab and cluster geometries have the advantage of the absence of a second defect. Therefore, spurious defect-defect interactions are avoided.

Nevertheless, even for a geometrically suitable slab or supercell, the CPU time may still be an issue in the case of *ab initio* calculations. Therefore, *ab initio* calculations are restricted by the available CPU power to special GBs of small Σ values and rather small interface reconstructions. Interfaces of arbitrary misorientation and/or GBs with impurities at the dilute limit would require systems consisting of at least a few thousands of atoms. In this case atomistic simulations, *i.e.* simulation techniques and models where atoms are the building blocks of the systems under consideration, are necessary. The actual form of the mostly empirically determined inter-atomic potential depends on the type of the studied system. Probably the most famous potentials are those suggested by Lennard-Jones (see, *e.g.*, [158,159]), Keating [160], Tersoff [161–164], Stillinger-Weber [165], and Finnis-Sinclair [166], as well as, *e.g.*, the embedded atom method [167–169], the bond-order potentials (see, *e.g.*, [170–174]), and indeed many other types. Inter-atomic empirical potentials have much lower demands on both CPU power and memory requirements. Calculations of systems consisting of a few millions of atoms and in a time scale of 10^{-9} of second are feasible nowadays. As example, the results simulated for Al are shown in fig. 10. For the $\Sigma 3\{111\}(\{1\text{-}12\})$ GBs which correspond to inclination angles of 0° and 90°, respectively, supercells consisting of a few hundreds of atoms are sufficient to provide converged boundary energies. However, for arbitrary inclination angles, supercells consisting of a few tens of thousands of atoms are necessary in order to obtain converged boundary energies.

Inter-atomic empirical potentials have been and are successfully used for studying various systems ranging from atoms and small molecules and clusters to large biomolecules, crystals, surfaces, interfaces, or liquid systems. However, the empirical potentials have also certain materials properties inherently included: They are parameterized and fitted to reproduce certain material properties such as lattice parameters, elastic constants, cohesive energies, or melting temperatures, just to mention a few. The transferability of a given potential, *i.e.* the ability of the potential to describe various environments, is always a question which should be carefully addressed (see, *e.g.*, [175]). Moreover, not all potentials are suitable for all systems: A nobel gas system may be accurately described by a Lennard-Jones or a Stillinger-Weber (SW) potential interaction may be suitable for tetrahedrally bonded covalent system. However, it is evident that a SW potential will probably fail to mimic a metallic system and many body potentials such as the Embedded Atom Method (EAM) or the bond order potentials may need to be employed. Hence, not only the parameterization but also the choice of potential depends strongly on the system under consideration.

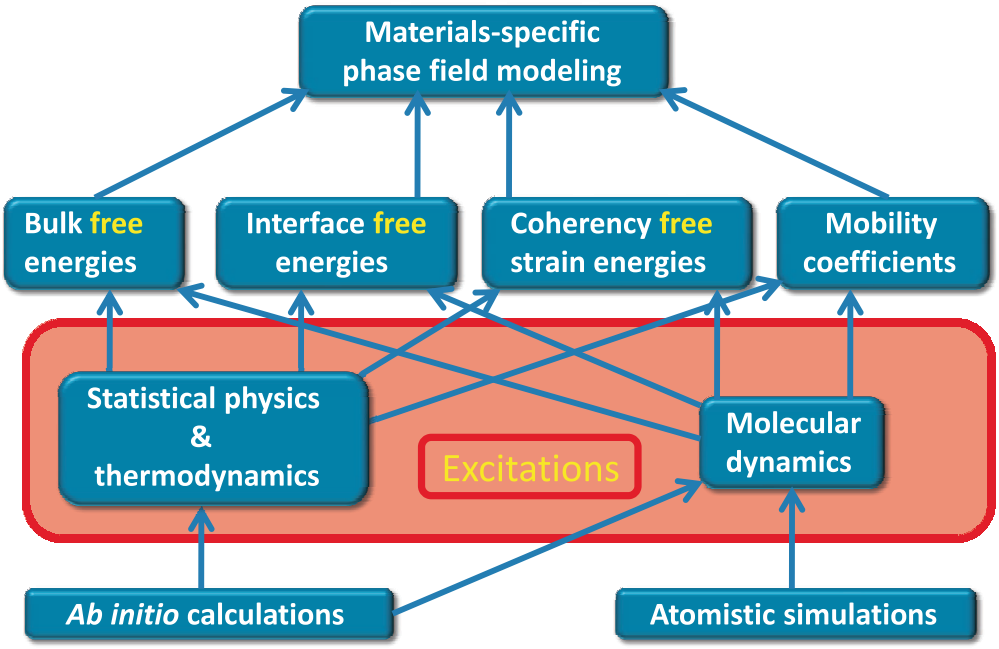

Fig. 11. Method-transfer of parameters within the multi-methodological scheme combining *ab initio*/atomistic calculations with the phase-field method.

A detailed review of quantum-mechanical and the inter-atomic empirical potential calculations is beyond the scope of the present review. Nevertheless, we should note here that first-principles calculations are currently restricted by the available computational power to describe special GB systems and/or systems consisting of only a few hundreds to few thousands of atoms, hence GBs of special misorientation and inclination. On the other hand, empirical or semi-empirical potentials may handle systems consisting of more than a few hundreds of thousands or even millions of atoms and they constitute a tool for robust and massive calculations [176] to explore the 5D configurational space of GBs. Nevertheless, their transferability and reliability must be carefully checked.

5.4 Electronic-structure methods interfacing phase-field simulations

The phase-field method has recently established itself as a powerful tool to predict microstructure evolution in many material systems (see, *e.g.*, [177–179]). It is a genuine representation of the original free-boundary problem in sharp-interface limit as the interface thickness reduces to zero. In the phase-field concept the interfacial conditions are avoided by introducing a set of smooth variables, the so-called phase-field variables, which characterize time and spacial evolutions of bulk phases in the underlying system. The thermodynamic and mathematical foundations underlying the phase-field method have been discussed in several recent review articles and monographs, see, *e.g.*, [180–186].

A prerequisite for phase-field simulations is the accurate knowledge of material specific parameters such as solid-solid and solid-liquid interface energies and the corresponding kinetic parameters (see schematics in fig. 11). In most cases this information is not always directly accessible in experiments. For example, the experimentally derived interfacial energies as well as interfacial mobilities are always influenced by small amounts of impurities: Even tiny concentrations of them may drastically alter the corresponding properties. In order to control the microstructural evolution, a detailed understanding of those phenomena is required. Thus, methods which will allow for a full control over all system parameters, such as interfacial symmetries, impurity concentrations, segregation effects, or pressure and temperature, are required. Atomistic calculations based on first-principles and/or empirical potentials satisfy the aforementioned requirements and are widely used to describe interfacial as well as interphasial phenomena.

Despite their clear suitability, quantum-mechanical and atomistic modeling tools also face a set of computational challenges when interfacing the phase-field methods. First, similarly as in case of FEM and FFT continuum methods, the complex grain boundary problem is present whenever solid-solid interfaces are involved. Second, any successful scheme combining quantum-mechanical/atomistic modeling with the phase-field method to describe solidification (or a non-crystalline phase) also requires the knowledge of solid-liquid interface properties. In contrast to the GB complexity that is characterized by a huge *static* configurational space, the solid-liquid interface simulations are typically rather lengthy and *dynamic* and thus computationally very demanding as well. A detailed discussion on the methods to

calculate solid-liquid interfacial energies and kinetic parameters can be found in the extensive and comprehensive review by Hoyt *et al.* in ref. [187] or in a recent review article [157]. Third, also in contrast to typical FFT or FEM simulations, the phase-field modeling often requires the knowledge of kinetic materials parameters, such as diffusion coefficients of all components in all present phases. Lastly, as a challenge that has not been fully recognized until recently, local stresses and strains in solid phases should be studied and their impact on the studied properties should be determined. The last issue is the topic of the next subsection.

5.5 Phase-field simulations including elastic strains

The role of the elastic stresses can be demonstrated on the shape of the precipitating particles. In the absence of stress, particles minimize the surface area for the given particle volume and become nearly spherical. In contrast, when the anisotropic elastic stresses are large, the surface energy yields to the stress, and the morphology of particles changes from spherical to cuboidal or elongated shapes such as rectangular or square plates [188]. The changes in particle morphology originate from the fact that the system is governed by two competing energies, i) one due to the presence of an interface and ii) the second one due to the elastic stresses. If only the interfacial energy is present, an isolated precipitate having isotropic surface energy takes a spherical shape to minimize the interfacial area. When an elastic stress is present, the total energy of the system may be reduced if the shape of the precipitate deviates from the spherical one. Specifically, if there is an anisotropy in the elastic constants, the interface tends to become flat along the elastically soft directions and highly curved along the elastically hard directions. The resulting shapes are cuboidal with rounded corners and nearly flat sides. The energy may be further reduced by changing the aspect ratio of the precipitate, resulting in the plate-like shapes. Such microstructures are seen in many alloy systems, *e.g.*, binary alloys Ni-Al [189] and Ni-Si [190,191]. The exact shape depends on the ratio of the two energies and the degree of the elastic anisotropy of the material. The subject has been widely reviewed in [192,193,177].

Elastic phase-field models for solid-solid materials interface dynamics can widely be found in the literature, see, *e.g.*, the contributions in [194]. For solid-liquid, respectively, solid-vapor systems a smaller amount of phase-field models including elastic mechanisms systematically can be found. An elastic phase-field model, which is capable to include the elastic energy and elastic misfit in epitaxial growth, has been developed in [195]. It has been adopted to eutectic growth by Ebrahimi in [196]. There it was assumed that the free energy of the system consists of a chemical free energy based on previous models for multiphase and two-phase growth [197–200] and an elastic free energy that includes the misfit stress between eutectic lamellae. Since the misfit stresses and strains arising during the eutectic solidification would relax in the liquid, the study of the influence of elastic interactions on eutectic growth is relevant only in solid-solid interactions, where the alloy is completely solidified. On the other hand, in real material systems grains typically have different orientations. Therefore, the orientation free energy has to be included into the elastic model of ref. [196] to assess the influence of the misfit stresses on eutectic growth in the case of solid-solid interactions. This model can be applied to simulate more realistic growth in Ti-Fe systems such as those observed in refs. [201–203].

Further, as far as the crystal growth with different orientations is concerned as another challenging issue, several phase-field models have also been already developed [205,206]. The first model is based on the work of Kobayashi *et al.* [207], where a non-conserved orientation field was introduced to specify the orientation of crystals, whereas the solid-liquid phases were distinguished with a single phase-field variable. This method has been applied more recently by Warren *et al.* to model polycrystalline materials [208]. Similar free energies are used by Gránásy *et al.* to establish the nucleation and growth in binary alloys [209].

Recently, Ebrahimi *et al.* [210] adopted the previous elastic phase-field model [196] to the growth of multiple eutectic nuclei with arbitrary orientations and then applied it to eutectic growth in Ti-Fe system. To satisfy different orientations, the orientation field and orientation energy for binary crystal nucleation was formulated as proposed in ref. [209] and for polycrystalline eutectic nucleation in ref. [211]. This extended model was then used to investigate the free growth of a limited number of eutectic nuclei and to examine the influence of orientation free energies on elastic fields and the resulting microstructure. The growth of three eutectic nuclei was simulated in a Ti-Fe system employing the following set of experimental parameters, (*e.g.*, from the CALPHAD database): molar volumes of phases, solid-liquid interface energies, equilibrium concentrations, kinetic coefficients, diffusion constants in the liquid phase, liquidus slopes, reference temperature, reference concentration at T_{R}, latent heats of fusion per unit volume, anisotropy terms, segregation coefficients, a pulling speed (directional growth) or thermal gradient (directional growth).

The simulated microstructures (see figs. 12(a),(b)) are in excellent agreement with the eutectic colonies (see fig. 12(c) and ref. [212]) observed in samples produced in cold-crucible casting [203]. A similar eutectic structure is described by Das *et al.* [204]. Other examples from the development of advanced structural and functional materials include high-strength ductile Ti-base i) nano-/ultrafine-eutectic-dendrite composites in Ti-Cu-Ni-Sn-X (X = Nb, Ta) [213–215] and ii) hypereutectic alloys by adding a third element like Ti-Fe-Co [202,216], Ti-Fe-(In, Nb) [217], Ti-Fe-Sn [218], Ti-Fe-Ga [219]. In all these cases, a bimodal grain size distribution of micrometer-size β-Ti dendrites embedded in a nano-/ultrafine-eutectic matrix is observed. Using the elastic phase-field model of Ebrahimi *et al.* [210] with misorientations, arbitrary phase diagrams of binary alloys as well as further growth phenomenas can be modeled.

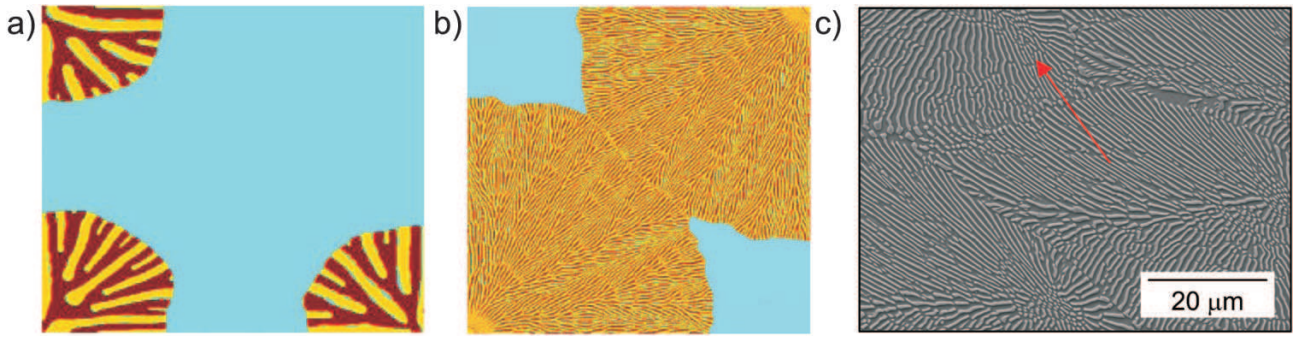

Fig. 12. Comparison of phase-field simulation results (a,b) with the detected microstructure of eutectic Fe-Ti alloys (c). The SEM picture (c) shows the microstructure of the $Ti_{70.5}Fe_{29.5}$ alloy prepared by arc-melting the pure elements with a purity of at least 99.99%. Samples were disk shaped samples (ingots) with a high of 0.8 cm and a diameter of about 3.5 cm. Due to previous studies [204] the cooling rate is about 10–40 K/s. The represented microstructure is taken from the upper part of the ingot. The image shows the round colonies with eutectic lamellae eutectic structure. Investigations revealing the coexistence of β-Ti(Fe) (A2, $Im\bar{3}m$) and the TiFe intermetallic phase (B2, $Pm\bar{3}m$). The heat-flow direction is indicated by the red arrow.

Consequently, this model can be proved to be a powerful tool to simulate the formation of colonies and eutectic growth in binary alloys with elastic interactions. However, for more detailed and accurate simulations with several nuclei in real systems experimental data on misfit energies depending on the associated orientations of the nuclei are necessary.

It can be concluded that with the current computational sources an optimum strategy would be to probe the solid-liquid interface properties employing experimental techniques, use equilibrium thermodynamics and kinetics parameters from existing databases, (*e.g.*, CALPHAD, DICTRA) but use theoretical modeling tools for all those parameters that are difficult to measure and are therefore not tabulated. In particular, atomistic modeling might be used to determine grain boundary properties and first-principles calculations to evaluate the impact of elastic strains and stresses on both thermodynamic and elastic properties of the studied phases (see, *e.g.*, [220]). As far as an error propagation from quantum-mechanical calculations into the phase-field modeling is concerned, a systematic study needs to be performed.

6 Summary

To summarize, electronic-structure calculations and/or classical atomistic-modeling approaches are suitable and versatile tools which can provide accurate material-specific parameters necessary for state-of-the-art multi-methodological approaches to address materials science problems involving complex microstructures as well as their evolution. The importance of *ab initio* and atomistic approaches is closely linked to the fact that many input parameters needed for continuum methods can not be directly accessed by experiment. Moreover, in order to control the microstructural evolution, an insight and a deeper understanding of various phenomena at the atomic scale are required. Fortunately, recent methodological developments and subsequent multi-methodological studies clearly indicate that both sub-atomic and atomistic methods can be efficiently combined in a multi-disciplinary manner into multi-methodological computational schemes.

In order to do design and apply such complex modeling approaches, a number of hurdles must be overcome. First, there are intrinsic sources of systematic errors that are inherent to different types of *ab initio* computational schemes. Second, next to systematic errors, a variety of errors related to computed atomistic models that represent real systems need careful analysis and control, specifically when interfacing *ab initio* calculations with other methods. Third, the major advantage of first-principles calculations to be free of empirical or fitting parameters (which makes them easily transferable into different environment and/or applicable to multicomponent alloys) comes at the price of extensive computational requirements. This restricts them to rather small system sizes ranging up to a few nanometers. In contrast, the parameters required by continuum methods are often associated with multi-species systems, long time evolutions of large systems and/or huge configurational spaces. All these aspects render the direct application of first-principles simulations to be computationally impossible for realistic systems. Complementarily to electronic-structure methods, the atomistic modeling can be extended to larger length and time scales but its transferability and accuracy should always be carefully checked and ensured in advance. Lastly, there is still a variety of methodological challenges, as, *e.g.*, multidimensional phase space of the interfacial misorientation degrees of freedom, suitable driving forces, and/or large length and time scales, that must be tackled. As the present report shows, the state-of-the-art modeling approaches systematically address these problems and the perspectives to find suitable solutions are very encouraging.

Financial support of the collaborative research center SFB 761 "Stahl *ab initio*" and the project "Scale-bridging studies of the elastic contributions to nucleation and initial micro-structure formation in the eutectic system Ti-Fe" of the Deutsche Forschungsgemeinschaft are gratefully acknowledged. Funding by the Interdisciplinary Centre for Materials Simulation (ICAMS), which is supported by ThyssenKrupp AG, Bayer MaterialScience AG, Salzgitter Mannesmann Forschung GmbH, Robert Bosch GmbH, Benteler Stahl/Rohr GmbH, Bayer Technology Services GmbH and the state of North-Rhine Westphalia as well as the European Commission in the framework of the European Regional Development Fund (ERDF) is also acknowledged. The research was partly funded through the "Triple-M Max-Planck Initiative on multiscale Materials Modeling of Condensed Matter".

References

1. P. Hohenberg, W. Kohn, Phys. Rev. B **136**, 864 (1964).
2. W. Kohn, L.J. Sham, Phys. Rev. A **140**, 1133 (1965).
3. J.P. Perdew, S. Kurth, Lect. Notes Phys., Vol. **620** (Springer, Berlin Heidelberg, 2003) p. 1.
4. K. Capelle, Braz. J. Phys. **36**, 1318 (2006).
5. S. Baroni, S. de Gironcoli, P.G.A. Dal Corso, Rev. Mod. Phys. **73**, 515 (2001).
6. R.M. Dreizler, E.K.U. Gross, *Density Functional Theory* (Springer-Verlag, Berlin, 1990).
7. R.G. Parr, W. Yang, *Density Functional Theory of Atoms and Molecules* (Oxford, New York, 1989).
8. W. Koch, M.C. Holthausen, *A Chemist's Guide to Density Functional Theory* (Wiley-VCH, Weinheim, 2000).
9. G. Grimvall, Sci. Model. Simul. **15**, 5 (2008).
10. G. Grimvall, Sci. Model. Simul. **15**, 21 (2008).
11. G. Grimvall, Sci. Model. Simul. **15**, 41 (2008).
12. M. Friák, W. Counts, D. Raabe, J. Neugebauer, Phys. Status. Solidi. b **245**, 2636 (2008).
13. N.D. Mermin, Phys. Rev. A **137**, 1441 (1965).
14. R. Kikuchi, Phys. Rev. **81**, 988 (1951).
15. R. Kikuchi, Calphad **26**, 33 (2002).
16. J.M. Sanchez, F. Ducastelle, D. Gratias, Physica A **128**, 334 (1984).
17. A. van de Walle, M. Asta, Acta Mater. **56**, 3202 (2008).
18. A. van de Walle, G. Ceder, Rev. Mod. Phys. **74**, 11 (2002).
19. A. Zunger, V. Blum, Phys. Rev. B **70**, 155108 (2004).
20. A. Ruban, I. Abrikosov, Rep. Prog. Phys. **71**, 046501 (2008).
21. A. van de Walle, M. Asta, Model. Simul. Mater. Sci. Eng. **10**, 521 (2002).
22. Y.S. Touloukian, E.H. Buyco, *Specific heat - metallic elements and alloys*, in *Thermophysical Properties of Matter*, Vol. **4** (IFI, Plenum, New York, 1970).
23. H. Hellmann, *Einführung in die Quantenchemie* (Deuticke, Leipzig, 1937).
24. R. Feynman, Phys. Rev. **56**, 340 (1939).
25. J. Harris, R.O. Jones, J.E. Müller, J. Chem. Phys. **75**, 3904 (1981).
26. P.E. Blöchl, Phys. Rev. B **50**, 17953 (1994).
27. B. Grabowski, T. Hickel, J. Neugebauer, Phys. Rev. B **76**, 024309 (2007).
28. L. Kaufman, H. Bernstein, *Computer Calculation of Phase Diagrams* (Academic, New York, 1970).
29. B. Grabowski, L. Ismer, T. Hickel, J. Neugebauer, Phys. Rev. B **79**, 134106 (2009).
30. B. Hallstedt *et al.*, Calphad **34**, 129 (2010).
31. J.P. Perdew, K. Burke, M. Ernzerhof, Phys. Rev. Lett. **77**, 3865 (1996).
32. J. Perdew *et al.*, Phys. Rev. Lett. **100**, 136406 (2008).
33. J.Z. Liu, A. van de Walle, G. Ghosh, M. Asta, Phys. Rev. B **72**, 144109 (2005).
34. G. Ghosh, S. Delsante, G. Borzone, M. Asta, R. Ferro, Acta Mater. **54**, 4977 (2006).
35. G. Ghosh, S. Vaynman, M. Asta, M.E. Fine, Intermetallics **15**, 44 (2007).
36. B.-Y. Tang, N. Wang, W.-Y. Yu, X.-Q. Zeng, W.-J. Ding, Acta Mater. **56**, 3353 (2008).
37. D. Raabe, B. Sander, M. Friák, D. Ma, J. Neugebauer, Acta Mater. **55**, 4475 (2007).
38. D. Ma, M. Friák, D. Raabe, J. Neugebauer, F. Roters, Phys. Status. Solidi. b **245**, 2642 (2008).
39. W. Counts, M. Friák, C. Battaile, D. Raabe, J. Neugebauer, Phys. Status. Solidi. b **245**, 2630 (2008).
40. W. Counts, M. Friák, D. Raabe, J. Neugebauer, Acta Mater. **57**, 69 (2009).
41. W. Counts, M. Friák, D. Raabe, J. Neugebauer, in *Magnesium, 8th International Conference on Magnesium Alloys and their Applications*, edited by K.U. Kainer (WILEY-VCH, Weinheim, Germany, 2009) p. 133.
42. W.A. Counts, M. Friák, D. Raabe, J. Neugebauer, Adv. Eng. Mat. **12**, 572 (2010).
43. W.A. Counts, M. Friák, D. Raabe, J. Neugebauer, Adv. Eng. Mat. **12**, 1198 (2010).
44. S. Nikolov *et al.*, *Proceedings of the fourth international conference on multiscale materials modeling (mmm-2008), tackling materials complexities via computational science* (2008) p. 667.
45. S. Nikolov *et al.*, Adv. Mater. **22**, 519 (2010).
46. S. Nikolov *et al.*, J. Mech. Behav. Biomed. Mater. **4**, 129 (2011).
47. P. Elstnerová *et al.*, Acta Biomater. **6**, 4506 (2010).
48. H. Fabritius *et al.*, *Chitin, topics in geobiology*, Vol. **34** (Springer Science and Business Media B.V., 2011) pp. 34–60.

49. J. von Pezold, A.D.M. Friák, J. Neugebauer, Phys. Rev. B **81**, 094203 (2010).
50. H.Y. Geng, M.H.F. Sluiter, N.X. Chen, Phys. Rev. B **72**, 014204 (2005).
51. E.S. Tasci, M.H.F. Sluiter, A. Pasturel, P. Villars, Acta Mater. **58**, 449 (2010).
52. A. Pasturel, E.S. Tasci, M.H.F. Sluiter, N. Jakse, Phys. Rev. B **81**, 140202(R) (2010).
53. A. Zunger, S.-H. Wei, L.G. Ferreira, J.E. Bernard, Phys. Rev. Lett. **65**, 353 (1990).
54. A. van de Walle, G. Ceder, J. Phase Equilib. **348**, 348 (2002).
55. S. Wei, L. Ferreira, J. Bernard, A. Zunger, Phys. Rev. B **42**, 9622 (1990).
56. L. Chen, D. Holec, Y. Du, P.H. Mayrhofer, Thin Solid Films **519**, 5503 (2011).
57. B. Alling *et al.*, Phys. Rev. B **75**, 045123 (2007).
58. D. Holec *et al.*, Phys. Rev. B **83**, 165122 (2011).
59. D. Holec, R. Franz, P. Mayrhofer, C. Mitterer, J. Phys. D: Appl. Phys. **43**, 145403 (2010).
60. D. Holec, F. Rovere, P.H. Mayrhofer, P.B. Barna, Scr. Mater. **62**, 349 (2010).
61. F. Rovere, D. Music, J. Schneider, P. Mayrhofer, Acta Mater. **58**, 2708 (2010).
62. M. Friák *et al.*, *Advanced intermetallic-based alloys for extreme environment and energy applications*, Vol. **1128**, p. 59, Mater. Res. Soc. Symp. Proc., Vol. **1124** (MRS, Warrendale, PA, 2009).
63. M. Friák, J. Deges, R. Krein, G. Frommeyer, J. Neugebauer, Intermetallics **18**, 1310 (2010).
64. A. Dick, T. Hickel, J. Neugebauer, Steel Res. Int. **80**, 603 (2009).
65. J.Z. Liu, A. van de Walle, G. Ghosh, M. Asta, Phys. Rev. B **72**, 144109 (2005).
66. A. van de Walle, Nat. Mater. **7**, 455 (2008).
67. K. Chen, L.R. Zhao, J.S. Tse, J. Appl. Phys. **93**, 2414 (2003).
68. F.D. Murnaghan, Proc. Natl. Acad. Sci. U.S.A. **30**, 244 (1944).
69. A.V. Hershey, J. Appl. Mech. **9**, 49 (1954).
70. H.M. Ledbetter, J. Appl. Phys. **44**, 1451 (1973).
71. R. Hill, Proc. Phys. Soc. London **65**, 350 (1952).
72. J.J. Gilvarry, Phys. Rev. **103**, 1701 (1956).
73. Y. Zhang, V. Blum, K. Reuter, Phys. Rev. B **75**, 235406 (2007).
74. W. Voigt, *Lehrbuch der Kristallphysik* (Teubner, Stuttgart, 1928).
75. A. Reuss, Z. Angew. Math. Mech. **9**, 49 (1929).
76. D. Raabe, Z. Zhao, F. Roters, Scr. Mater. **50**, 1085 (2004).
77. D. Raabe, Z. Zhao, W. Mao, Acta Mater. **50**, 4379 (2002).
78. D. Raabe, M. Sachtleber, Z. Zhao, D. Raabe, Mater. Sci. Eng. A **336**, 81 (2002).
79. D. Raabe, P. Klose, B. Engl, K.-P. Inlau, F. Friedel. F. Roters, Adv. Eng. Mater. **4**, 169 (2002).
80. F. Roters, P. Eisenlohr, L. Hantcherli, D.D. Tjahjanto, T.R. Bieler, D. Raabe, Acta Mater. **58**, 1152 (2010).
81. F. Roters, P. Eisenlohr, T.R. Bieler, D. Raabe, *Crystal Plasticity Finite Element Methods in Materials Science and Engineering* (Wiley-VCH Weinheim, 2010).
82. H. Pi, J. Han, C. Zhang, A.K. Tieu, Z.Y. Jiang, Adv. Mater. Res. **15-17**, 935 (2007).
83. G.I. Taylor, J. Inst. Met. **62**, 307 (1938).
84. R. Hill, J.R. Rice, J. Mech. Phys. Solids **20**, 401 (1972).
85. R.J. Asaro, J. Appl. Mech. **50**, 921 (1983).
86. Z. Zhao, F. Roters, W. Mao, D. Raabe, Adv. Eng. Mater. **3**, 984 (2001).
87. H. Moulinec, P. Suquet, C. R. Acad. Sci. Paris II **318**, 1417 (1994).
88. H. Moulinec, P. Suquet, Comput. Meth. Appl. Mech. Eng. **157**, 69 (1998).
89. R.A. Lebensohn, Acta Mater. **49**, 2723 (2001).
90. R. Lebensohn, Y. Liu, P.P. Castaneda, Proc. R. Soc. London Ser. A **460**, 1381 (2004).
91. R. Lebensohn, R. Brenner, O. Castelnau, A. Rollett, Acta Mater. **56**, 3914 (2008).
92. R. Lebensohn *et al.*, Acta Mater. **57**, 1405 (2009).
93. A.D. Rollett *et al.*, Model. Simul. Mater. Sci. Eng. **18**, 074005 (2010).
94. S.-B. Lee, J. Rickman, A. Rollett, Acta Mater. **55**, 615 (2010).
95. S.-B. Lee, R.A. Lebensohn, A. Rollett, Int. J. Plast. **27**, 707 (2011).
96. R. Janisch, N. Ahmed, A. Hartmaier, Phys. Rev. B **81**, 184108 (2010).
97. R. Janisch, C. Elsasser, Int. J. Mater. Res. **100**, 1488 (2009).
98. A. Bohner, R. Janisch, A. Hartmaier, Scripta Mater. **60**, 504 (2009).
99. E. Hristova, R. Janisch, R. Drautz, A. Hartmaier, Comput. Mater. Sci. **50**, 1088 (2011).
100. M. Prechtel, P.L. Ronda, R. Janisch, A. Hartmaier, G. Leugering, P. Steinmann, Int. J. Fract. **168**, 15 (2011).
101. M. Friák, M. Šob, Phys. Rev. B **77**, 174117 (2008).
102. N. Nagasako, M. Jahnatek, R. Asahi, J. Hafner, Phys. Rev. B **81**, 094108 (2010).
103. D. Legut, M. Friák, M. Šob, Phys. Today **61**, 10 (2008) Replay.
104. S. Ogata, J. Li, J. App. Phys. **106**, 113534 (2009).
105. M. Šob, M. Friák, Intermetallics **17**, 523 (2009).
106. M. Jahnatek, J. Hafner, M. Krajci, Phys. Rev. B **79**, 224103 (2009).
107. D. Legut, M. Friák, M. Šob, Phys. Rev. B **81**, 214118 (2010).
108. J. Zhang, Y. Yang, K. Xu, V. Ji, Comput. Mat. Sci. **43**, 917 (2008).
109. D. Legut, M. Friák, M. Šob, Phys. Rev. Lett. **99**, 016402 (2007).

110. J. Zhang, Y. Yang, K. Xu, V. Ji, Can. J. Phys. **86**, 935 (2008).
111. M. Šob, M. Friák, L. Wang, V. Vitek, Key Eng. Mater. **227**, 261 (2002).
112. H. Wang, M. Li, J. Phys. Cond. Mat. **22**, 295405 (2010).
113. M. Friák, M. Šob, V. Vitek, Phys. Rev. B **63**, 052405 (2001).
114. Y. Liu, Y. Zhang, R. Hong, G. Lu, Chin. Phys. B **18**, 1923 (2009).
115. M. Friák, A. Schindlmayr, M. Scheffler, New J. Phys. **9**, 5 (2007).
116. Y. Liu, H. Zhou, Y. Zhang, S. Jin, G. Lu, Nucl. Instrum. Methods Phys. Res. B **18**, 3282 (2009).
117. M. Šob, M. Friák, D. Legut, J. Fiala, V. Vitek, Mat. Sci. Eng. A **387-389**, 148 (2004).
118. P. Šesták, M. Černý, J. Pokluda, Mat. Sci. Eng. A **481-482**, 247 (2008).
119. M. Černý, J. Pokluda, Acta Mater. **58**, 3117 (2010).
120. J. Pokluda, M. Černý, J. Šandera, M. Šob, J. Computer-Aided Mater. Design **11**, 1 (2004).
121. M. Černý, M. Šob, J. Pokluda, J. Šandera, J. Phys.: Condens. Matter **16**, 1045 (2004).
122. M. Šob, M. Friák, L. Wang, V. Vitek, *Proceedings of the International Conference on Solid-Solid Phase Transformations '99 (jimic-3)* (The Japan Institute of Metals, Sendai, 1999) pp. 855–858.
123. J. Wang, J. Zhang, K. Xu, Crys. Res. Tech. **44**, 184 (2009).
124. M. Friák, M. Šob, V. Vitek, Phys. Rev. B **68**, 184101 (2003).
125. J. Bhattacharya, A.V. der Ven, Acta Mater. **56**, 4226 (2008).
126. M. Černý, J. Pokluda, M. Šob, M. Friák, J. Šandera, Phys. Rev. B **67**, 035116 (2003).
127. M.J. Mehl, D. Finkenstadt, Phys. Rev. B **77**, 052102 (2008).
128. M. Friák, M. Šob, V. Vitek, Phil. Mag. **83**, 3529 (2003).
129. H. Djohari, F. Milstein, D. Maroudas, Appl. Phys. Lett. **90**, 161910 (2007).
130. M. Friák, M. Šob, V. Vitek, *High-Temperature Ordered Intermetallic Alloys ix, MRS Symp. Proc.*, Vol. **646**, (Materials Research Society, Warrendale, 2001) p. N.4.8.1.
131. Y. Liu, Y. Zhang, H. Zhou, G. Lu, M. Kohyama, J. Phys. Cond. Mat. **20**, 335216 (2008).
132. M. Šob, M. Friák, L. Wang, V. Vitek, *Computational Modeling of Materials, Minerals, and Metals Processing* (The Minerals, Metals and Materials Society, Warrendale, PA, 2001) pp. 715–724.
133. N. Nagasako, M. Jahnatek, R. Asahi, J. Hafner, Phys. Rev. B **81**, 094108 (2010).
134. M. Jahnatek, M. Krajci, J. Hafner, Phys. Rev. B **76**, 014110 (2007).
135. M. Šob, M. Friák, L. Wang, V. Vitek, *Multiscale Modeling of Materials, MRS Symp. Proc.*, Vol. **538**, (Materials Research Society, Pittsburgh, 1999) pp. 523–527.
136. R. Zhang, S. Sheng, S. Veprek, Appl. Phys. Lett. **91**, 031906 (2007).
137. M. Šob, M. Friák, L. Wang, V. Vitek, *Proceedings of the 1st Meeting of the Molecular Dynamics Committee of the Japanese Society of Materials*, 48th period (Japanese Society of Materials, Osaka, 1999) pp. 1–5.
138. X. Cui, J. Wang, X. Liang, G. Zhao, Chin. Phys. Lett. **27**, 027101 (2010).
139. M. Šob, M. Friák, D. Legut, V. Vitek, *Complex Inorganic Solids - Structural, Stability, and Magnetic Properties of Alloys* (Springer-Verlag, Berlin-Heidelberg-New York, 2005) pp. 307–326.
140. H. Zhou *et al.*, J. Phys. Cond. Mat. **21**, 175407 (2009).
141. M. Friák, M. Šob, V. Vitek, *Electron Correlations and Materials Properties 2*, (Kluwer Academic/Plenum Publishers, NY, 2003) pp. 399–415.
142. G. Xu *et al.*, Chin. Phys. Lett. **26**, 046302 (2009).
143. D. Legut, M. Šob, *Materials Structure and Micromechanics of Fracture v and Book Series*, Vol. **567-568** (Materials Science Forum, 2008) pp. 77–80.
144. R. Zhang, D. Legut, R. Niewa, A. Argon, S. Veprek, Phys. Rev. B **82**, 104104 (2010).
145. M. Černý, J. Pokluda, J. Phys. Condens. Matter **21**, 145406 (2009).
146. M. Černý, J. Pokluda, Mater. Sci. Eng. A **483-484**, 69 (2008).
147. M. Černý, J. Pokluda, Mater. Sci. Forum **56-59**, 73 (2008).
148. M. Černý, J. Pokluda, Comput. Mater. Sci. **44**, 127 (2008).
149. M. Černý, Mater. Sci. Eng. A **462**, 432 (2008).
150. M. Černý, R. Boyer, M. Šob, S. Yip, J. Computer-Aided Mater. Design **12**, 161 (2005).
151. M. Zelený, D. Legut, M. Šob, Phys. Rev. B **78**, 224105 (2008).
152. M. Zelený, M. Šob, Phys. Rev. B **77**, 155435 (2008).
153. M. Zelený, M. Šob, J. Hafner, Phys. Rev. B **79**, 134421 (2009).
154. M. Zelený, M. Friák, M. Šob, Phys. Rev. B **83**, 184424 (2011).
155. M. Friák, T. Hickel, A. Udyansky, A. Dick, J. von Pezold, O. Kim, W.A. Counts, M. Šob, T. Gebhardt, D. Music, J. Schneider, D. Raabe, J. Neugebauer, Steel Res. Int. **82**, 86 (2010).
156. C.-S. Kim, A. Rollett, G. Rohrer, Scripta Mater. **54**, 1005 (2006).
157. L. Lymperakis, M. Friák, J. Neugebauer, Eur. Phys. J. ST **177**, 41 (2009).
158. S. Erkoc, Phys. Rep. **278**, 79 (1997).
159. R.M. Nieminen, M.J. Puska, M.J. Manninen, *Many-Atom Interactions in Solids, Proceedings in Physics*, Vol. **48** (Springer, Berlin, Heidelberg, 1990).
160. P.N. Keating, Phys. Rev. **145**, 637 (1966).
161. J. Tersoff, Phys. Rev. Lett. **56**, 632 (1986).
162. J. Tersoff, Phys. Rev. B **38**, 9902 (1988).

163. J. Tersoff, Phys. Rev. Lett. **61**, 2879 (1988).
164. J. Tersoff, Phys. Rev. B **39**, 5566 (1989).
165. F. Stillinger, T. Weber, Phys. Rev. B **31**, 5262 (1985).
166. M.W. Finnis, *Interatomic Forces in Condensed Matter* (Oxford University Press, London, 2003).
167. M.S. Daw, M. Baskes, Phys. Rev. B **29**, 6443 (1994).
168. M.S. Daw, S. Foiles, Mat. Sci. And Engr. Rep. **9**, 251 (1993).
169. R.R. Zope, Y. Mishin, Phys. Rev. B **68**, 024102 (2003).
170. R. Drautz, D.G. Pettifor, Phys. Rev. B **74**, 174117 (2006).
171. T. Hammerschmidt, R. Drautz, D.G. Pettifor, Int. J. Mater. Res. **100**, 1479 (2009).
172. T. Hammerschmidt, P. Kratzer, M. Scheffler, Phys. Rev. B **81**, 159905 (2010).
173. K.A. Fichthorn, Y. Tiwary, T. Hammerschmidt, P. Kratzer, M. Scheffler, Phys. Rev. B **83**, 195328 (2011).
174. B. Seiser, T. Hammerschmidt, A.N. Kolmogorov, R. Drautz, D.G. Pettifor, Phys. Rev. B **83**, 224116 (2011).
175. A.I. Duff, M.H.F. Sluiter, Mater. Trans. **51**, 675 (2010).
176. B. Lee, S. Choi, Modeling Simul. Mater. Sci. Eng. **12**, 621 (2004).
177. P. Fratzl, O. Penrose, J. Lebowitz, J. Stat. Phys. **95**, 1429 (1999).
178. J.A.K. Thornton, P.W. Voorhees, Acta. Mater. **51**, 5675 (2003).
179. N. Moelans, B. Blanpaina, P. Wollantsa, Calphad **32**, 268 (2008).
180. W. Boettinger, J. Warren, C. Beckermann, A. Karma, Annu. Rev. Mater. Res. **32**, 163 (2002).
181. L. Chen, Annu. Rev. Mater. Res. **32** (2002).
182. M. Plapp, J. Cryst. Growth **303**, 49 (2007).
183. I. Singer-Loginova, H. Singer, Rep. Prog. Phys. **71**, 106501 (2008).
184. I. Steinbach, Model. Simul. Mater. Sci. Eng. **17**, 073001 (2009).
185. H. Emmerich, Adv. Phys. **57**, 1 (2008).
186. H. Emmerich, *The Diffuse Interface Approach in Material Science - Thermodynamic Concepts and Applications of Phase-Field Models, Habilitation*, Lect. Notes Phys., Vol. **73** (Springer, Berlin, 2003).
187. M. Asta, J. Hoyt, Acta Mater. **48**, 1089 (2000).
188. V. Vaithyanathan, L. Chen, Acta Mater. **50**, 4031 (2002).
189. A. Ardell, R. Nicholson, Acta Metall. **14**, 1295 (1966).
190. J. Cho, A. Ardell, Acta Mater. **45**, 1393 (1997).
191. J. Cho, A. Ardell, Acta Mater. **46**, 5907 (1998).
192. M. Doi, Mater. Trans. JIM,336371992.
193. P. Voorhees, Annu. Rev. Mater. Sci. **22**, 197 (1992).
194. H. Emmerich, Philos. Mag. **90**, 1495 (2010).
195. H. Emmerich, Cont. Mech. Thermodynamics **15**, 197 (2003).
196. Z. Ebrahimi, J.L. Rezende, J. Kundin, in preparation (2011).
197. R. Folch, M. Plapp, Phys. Rev. E **72**, 011602 (2005).
198. B. Echebarria, R. Folch, A. Karma, M. Plapp, Phys. Rev. E **70**, 061604 (2004).
199. J. Tiaden, B. Nestler, H. Diepers, I. Steinbach, Physica D **115**, 73 (1998).
200. S.G. Kim, W. Kim, T. Suzuki, Phys. Rev. E **60**, 7186 (1999).
201. J. Das, K.B. Kim, F. Baier, W. Löser, J. Eckert, Appl. Phys. Lett. **87**, 161907 (2005).
202. D.V. Louzguine, H. Kato, J. Mater. Res. **19**, 3600 (2004).
203. J. Das, K. Kim, W. Xu, W. Löser, J. Eckert, Mater. Sci. Eng. A **449**, 737 (2007).
204. J. Das, K. Kim, W. Xu, W. ö, J. Eckert, Mat. Sci. Eng. A **449-451**, 737 (2007) Proceedings of the 12th International Conference on Rapidly Quenched and Metastable Materials.
205. H. Assadi, *Solidification and Crystallization* (2004).
206. J. Hubert, PhD thesis (RWTH Aachen, 2009).
207. R. Kobayashi, J. Warren, W. Carter, Physica D **119**, 415 (1998).
208. J. Warren, R. Kobayashi, A. Lobkovsky, W. Carter, Acta. Mater. **51**, 6035 (2003).
209. L. Gránásy, T. Börzsönyi, T. Pusztai, Phys. Rev. E **88**, 206105 (2002).
210. Z. Ebrahimi, J.L. Rezende, R. Kumar, H. Emmerich, submitted to J. Phys.: Condens. Matter (2011).
211. D. Lewis, T. Pusztai, L. Gránásy, J. Warren, W. Boettinger, J. Met. **56**, 34 (2004).
212. A. Schlieter, U. Kühn, J. Eckert, W. Löser, T. Gemming, M. Fríak, J. Neugebauer, Intermetallics **19**, 327 (2011).
213. G. He, W. Löser, J. Eckert, Acta Mater. **51**, 5223 (2003).
214. G. He, J. Eckert, W. Löser, L. Schultz, Nature Mater. **2**, 33 (2003).
215. G. He, J. Eckert, W. Löser, M. Hagiwara, Acta Mater. **52**, 3035 (2004).
216. D.V. Louzguine-Luzgin, L.V. Louzguina-Luzgina, H. Kato, A. Inoue, Acta Mater. **53**, 2009 (2005).
217. D. Misra, S. Sohn, H. Gabrisch, W. Kim, D. Kim, Intermetallics **18**, 342 (2010).
218. G.A. Song, J.H. Han, T.E. Kim, J.M. Park, D.H. Kim, S. Yi, Y. Seo, N.S. Lee, K.B. Kim, Intermetallics **19**, 536 (2011).
219. D. Misra, S. Sohn, W. Kim, D. Kim, Intermetallics **18**, 254 (2010).
220. L.-F. Zhu, M. Fríak, A. Dick, B. Grabowski, T. Hickel, F. Liot, D. Holes, A. Schlieter, U. Kühn, J. Eckert, Z. Ebrahimi, H. Emmerich, J. Neugebauer, submitted to Acta Mater. (2011).